ANOMALOUS FLUX ENTRY INTO ANISOTROPIC SUPERCONDUCTORS

by

Michael Wayne Denhoff

B.Sc. University of Calgary, 1976

A THESIS SUBMITTED IN PARTIAL FULFILLMENT OF

THE REQUIREMENTS FOR THE DEGREE OF

MASTER OF SCIENCE

in the Department

of

Physics

SIMON FRASER UNIVERSITY

August 1981

APPROVAL

Name: Michael Wayne Denhoff

Degree: Master of Science

Title of a thesis: Anomalous Flux Entry into Anisotropic Superconductors

Examining Committee:

Chairperson: B. P. Clayman

Suso Gygax
Senior Supervisor

J. F. Cochran

M. Plischke

R. F. Frindt
External Examiner
Professor
Department of Physics
Simon Fraser University

Date Approved: 28 Aug/81

PARTIAL COPYRIGHT LICENSE

I hereby grant to Simon Fraser University the right to lend my thesis, project or extended essay (the title of which is shown below) to users of the Simon Fraser University Library, and to make partial or single copies only for such users or in response to a request from the library of any other university, or other educational institution, on its own behalf or for one of its users. I further agree that permission for multiple copying of this work for scholarly purposes may be granted by me or the Dean of Graduate Studies. It is understood that copying or publication of this work for financial gain shall not be allowed without my written permission.

Title of Thesis/Project/Extended Essay

Anomalous Flux Entry into Anisotropic Superconductors

Author:

(signature)

Michael Wayne Denhoff

(name)

13 Nov 1981

(date)

ABSTRACT

Flux entry into an anisotropic type II superconductor was investigated using magnetization measurements on single crystals of $NbSe_2$. Demagnetization effects were large and were taken into account quantitatively. Flux entry measurements were also performed on an isotropic superconductor, Nb 48 atomic % Ti, as a check on the experimental method. The measured critical flux entry fields for $NbSe_2$ were larger than the expected lower critical fields calculated using literature values of the upper critical field and anisotropic Ginzburg-Landau theory. For fields applied parallel to the crystal layers, the entrance field was found to have a small dependence on the crystal size. It is suggested that these observations could be explained using critical state theory. A plot of the critical entry field against the angle of the applied magnetic field with respect to the crystal c-axis, shows an anomalous cusp-like feature. This cusp is not explained for $NbSe_2$ by the anisotropic Ginzburg-Landau theory. It can be explained by assuming that, at the critical entrance field, the flux lines are not parallel to the magnetic field, but are either nearly parallel to or nearly perpendicular to the crystal layers depending on the direction of the applied field.

ACKNOWLEDGEMENTS

I would like to thank Dr. Jerome Long of Virginia Polytechnic Institute and State University who did much of the design and construction of the magnetometer. Discussions with Dr. R. A. Klemm of Iowa State University about the anisotropy of H_{c1} and the demagnetization problem have been helpful. I am indebted to Dr. R. F. Frindt and the members of his group, P. Joensen and G. Scholz, for supplying the $NbSe_2$ crystals. Finally, I thank my supervisor Dr. Suso Gygax for the freedom he allowed me in this research, while supplying constant, and much appreciated, guidance and councel.

TABLE OF CONTENTS

LIST OF TABLES

LIST OF FIGURES

I. Introduction

Anisotropic type II superconductors have been the object of much interest in recent years. There have been considerable theoretical and experimental investigations of the properties of anisotropic superconductors, in particular, the anisotropy of the upper critical field. Only recently, however, has there been a theoretical treatment of the lower critical field H_{c1}.[1] To date, there has not been an experimental determination of the anisotropy of H_{c1}[2]. The most commonly studied anisotropic superconductors are layered transition metal dichalcogenides. Crystals of these substances grow in the shape of platelets. A superconductor near H_{c1} is in a strongly diamagnetic state. Therefore, large demagnetizing effects due to the shape of these crystals complicate the measurement of H_{c1}.

Intimately connected with the lower critical field is the entry of magnetic flux into a superconductor. For applied fields above H_{c1} it is thermodynamically favorable for flux to enter a superconductor. But in a real superconductor, there can exist irreversible effects which oppose the movement of flux. This can delay the entrance of flux until an applied field somewhat larger than H_{c1} is reached. It is the entrance of flux into a superconductor which marks the transition from the fully diamagnetic (Meissner) state to the partly diamagnetic (mixed) state. The measurement of magnetization of a crystal can be used to determine the onset of flux entry which marks the phase change.

In Chapter II of this thesis, a theoretical description of an isotropic type II superconductor is given along with a derivation of the

value of H_{c1}. This is then generalized to include demagnetization effects. The theory developed by Klemm and Clem[1] for anisotropic superconductors is presented in the same way as the theory of the isotropic case. Finally, Chapter II gives a discussion of the possibility of delayed flux entry. Chapter III gives the construction details and operating principles of the magnetometer used to measure the magnetization of samples. In Chapter IV, flux entry measurements for an isotropic superconductor Nb48%Ti, are reported. These results are used as a check on demagnetization calculations and to investigate delayed flux entry for the isotropic case. The flux entry measurements for an anisotropic superconductor, $NbSe_2$, are given in Chapter V. Also in Chapter V, is a discussion of the experimental results and a comparison with theory. Chapter VI summarizes the work presented in this thesis and suggests some possible future work.

II. Theory

Isotropic Type II Superconductors

This section will use Ginzburg-Landau theory to show how to find the lower critical field H_{c1} of an isotropic type II superconductor. First H_{c1} will be found for a long cylinder parallel to an applied field, and then demagnetization effects will be taken into account. The first part of this calculation is done in any textbook covering type II superconductivity.[3,4]

Type II superconductors can be characterized by two lengths. Firstly, the coherence length ξ, which is the length scale over which the order parameter can vary. Secondly, the penetration depth λ, which is the length scale over which the microscopic magnetic field can vary. Both of these parameters have the same temperature dependence near T_c. This leads to the definition of the temperature independent parameter $\kappa=\lambda/\xi$, which is used to classify the behavior of a superconductor.

When a small magnetic field is applied to a type II superconductor, it will be in the Meissner state where the magnetic induction is zero in the bulk of the superconductor. The superconductor is now a perfect diamagnet with magnetization $M=-H/4\pi$. If the applied field is increased to the lower critical field H_{c1}, it will be energetically favorable for the superconductor to allow the entry of some magnetic flux. This marks the transition to the mixed state. The flux enters in the form of fluxoids. An isolated fluxoid can be modeled, for large κ, as a cylinder extending

through the superconductor in the direction of the applied field. The core of the fluxoid is in the normal state and has a radius of ξ. The microscopic magnetic field is at a maximum within the core. Shielding currents around the core cause the field to decrease, over a length scale λ, to zero in the superconducting bulk. The magnetic flux contained in a fluxoid, including both the core and the shielding current areas, is one quantum of magnetic flux ϕ. As the applied field is further increased more fluxoids enter the superconductor. When the applied field reaches the upper critical field H_{c2} the entire bulk of the superconductor makes a second order transition to the normal state.

A value for H_{c1} can be found by considering the Gibbs free energy per unit volume of the superconductor (in cgs units),[3]

$$g = nF_1 + \sum_{i>j} J_{ij} + \frac{B^2}{8\pi} - \vec{H}_a \cdot \vec{M} \quad . \qquad (1)$$

F_1 is the self-energy of a fluxiod. It consists of the lost condensation energy of the normal core plus the kinetic energy of the shielding supercurrents. n is the number of fluxoids per unit area. Since each fluxoid contains one quantum of flux, n can be expressed in terms of the average magnetic induction, $n=B/\phi$. The second term expresses the interaction energy between fluxoids. Near H_{c1} the distance between fluxoids is large compared to λ and the interaction term can be neglected. The third term is the energy density of a magnetic field. The final term gives the energy of a magnetized material in an externally applied field. The magnetization can be expressed as $4\pi M=B-H_i$, where H_i is the internal magnetic field. For a long cylinder parallel to H_a, $H_i=H_a$ and B will be parallel to H_a. Near H_{c1}, B will be small and terms in B^2 can be

neglected. The Gibbs energy near H_{c1} can then be written

$$g = \frac{B}{\phi_o} F_1 - \frac{H_a B}{4\pi} + \frac{H_a^2}{4\pi} \quad . \tag{2}$$

The Gibbs energy can be decreased for non-zero B, if

$$H_a > \frac{4\pi F_1}{\phi_o} \equiv H_{c1} \quad . \tag{3}$$

H_{c1} is the limit of H_a as B goes to zero. This defines the lower critical field H_{c1}. The self-energy of a fluxoid F_1 can be found using Ginzburg-Landau theory. One finds

$$4\pi F_1 = \frac{\phi_o H_c}{\sqrt{2}\,K} (\ln K + 0.497) \tag{4}$$

where H_c is the thermodynamical critical field.

For other shapes and orientations of a magnetic (superconducting) sample demagnetizing effects must be considered. The demagnetization problem can be solved analytically for a magnetic material in the shape of an ellipsoid, whose magnetization is given by $M=\chi H$. In this case H can be described by a scalar potential, $H=\nabla\phi$, and the scalar potential is the solution to Laplace's equation.[5,6,7] For a uniform applied field H_a, there will be a uniform field H_i inside the ellipsoid. If the coordinates are chosen along the symmetry axes of the ellipsoid, the components of the internal field are given by

$$\begin{aligned} H_{ix} &= \frac{H_{ax}}{1 + \chi L/4\pi} \\ H_{iy} &\quad \frac{H_{ay}}{1 + \chi M/4\pi} \\ H_{iz} &\quad \frac{H_{az}}{1 + \chi N/4\pi} \end{aligned} \tag{5}$$

where L, M, and N are geometrical demagnetization factors in the x, y, and z directions, respectively. The general expressions for the demagnetization factors include elliptic integrals and are quite complicated. In the case of an oblate spheroid with semiaxes a, b, and c in the x, y, and z directions, and where a=b>c the demagnetization factors are[6]

$$L = M = \frac{1}{2\left[\left(\frac{b}{c}\right)^2 - 1\right]} \left\{ \left(\frac{b}{c}\right)^2 \left[\left(\frac{b}{c}\right)^2 - 1\right]^{1/2} \cdot \arcsin\left(\frac{\left[\left(\frac{b}{c}\right)^2 - 1\right]^{1/2}}{b/c} \right) - 1 \right\}$$

$$N = \frac{(b/c)^2}{\left[\left(\frac{b}{c}\right)^2 - 1\right]} \left\{ 1 - \frac{1}{\left[\left(\frac{b}{c}\right)^2 - 1\right]^{1/2}} \cdot \arcsin\left(\frac{\left[\left(\frac{b}{c}\right)^2 - 1\right]^{1/2}}{b/c} \right) \right\} . \qquad (6)$$

Now, the applied critical field can be found for an oblate spheroid, with its short axis, c, in the z direction, for an arbitrary direction of the applied field. Starting from equation (2-1), neglecting the interacting term and the B^2 term, gives for the Gibbs energy

$$g = \frac{B}{\phi_o} F_i - \vec{H}_a \cdot \vec{M} \quad , \qquad (7)$$

where $\vec{M}$ depends on the internal field, so that

$$g = \frac{B}{\phi_o} F_i - \vec{H}_a \cdot \left[\frac{\vec{B}}{4\pi} - \frac{\vec{H}_i}{4\pi} \right] \quad . \qquad (8)$$

Substituting for $\vec{H}_i$ using equation (2-5) leads to

$$g = \frac{B}{\phi_o} F_i - \frac{\vec{H}_a}{4\pi} \cdot \left[\frac{\vec{B}}{1 - \overrightarrow{\overrightarrow{D}}} - \frac{\vec{H}_a}{1 - \overrightarrow{\overrightarrow{D}}} \right] \quad , \qquad (9)$$

where $\overrightarrow{\overrightarrow{D}}$ is the demagnetization tensor. It can be expressed as a diagonal matrix with L, M, and M as its diagonal elements. Doing the dot product and omitting terms independent on B gives

$$g = \frac{B}{\phi_o} F_i - \frac{H_{ax} B \sin\theta_B}{4\pi(1 - L)} - \frac{H_{az} B \cos\theta_B}{4\pi(1 - N)} \quad , \qquad (10)$$

where θ_B is the angle of B with respect to the z axis. (B is in the same direction as the fluxoids.) The Gibbs energy can be decreased by choosing B=0 when

$$\frac{H_{ax}\sin\theta_B}{4\pi(1-L)} + \frac{H_{az}\cos\theta_B}{4\pi(1-N)} > \frac{F_i}{\phi_o} \quad . \tag{11}$$

If θ_a is the angle between the applied field and the z axis, equation (2-11) can be solved to give H_a,

$$H_a > \frac{4\pi F_i/\phi_o}{\frac{\sin\theta_a \sin\theta_B}{1-L} + \frac{\cos\theta_a \cos\theta_B}{1-N}} \equiv H_{c1a} \quad . \tag{12}$$

The angle θ_B is still undetermined. It can be found by considering, for a fixed angle of the applied field, in which direction the first fluxoid lies, giving the smallest value of H_{c1}. In other words, minimizing H_{c1} with respect to θ_B, which gives

$$\tan\theta_B = \frac{1-N}{1-L}\tan\theta_a \quad . \tag{13}$$

The angle θ_i which the internal field H_i makes with respect to the z axis, can be found using equations (2-5) to be

$$\tan\theta_i = \frac{1-N}{1-L}\tan\theta_a \quad . \tag{14}$$

That is, for an isotropic superconductor the first flux line at H_{c1} enters in the direction parallel to the internal field. The applied critical field given by equation (2-12) is the same as using the internal critical field (equation (2-3)) transformed to the applied field using equations (2-5) and $\chi=-1/4\pi$.

Anisotropic Type II Superconductor

In this section an expression is found for H_{c1} for an anisotropic superconductor and the interesting features of this solution will be described.

The usual way to describe an anisotropic superconductor is to use an anisotropic effective electron mass in the Ginzburg-Landau theory.[1,8] Consider a layered substance with conducting layers in the x-y plane separated by van der Waals gaps. The effective mass in the z direction would be larger than in the x and y directions, $m_z > m_x = m_y$. The effective mass model is in good agreement with experimental results for the upper critical field.[9]

We found that the calculation of H_{c1} for an anisotropic superconductor can be done in the same way as the above calculation for an isotropic superconductor. The only difference is in the calculation of the self-energy of a fluxoid, $F_1(\theta_B)$. The self-energy will depend on the direction in which the fluxoid lies. This calculation is somewhat complicated. It has been done by R. A. Klemm and J. R. Clem.[1] Their result has the same form as the isotropic theory, but they use an anisotropic Ginzburg Landau parameter $\tilde{\kappa}$ given by

$$\tilde{\kappa} = \kappa_\perp \left[\cos^2\theta_B + \varepsilon \sin^2\theta_B\right]^{-1/2} , \qquad (15)$$

where $\kappa_\perp = \kappa(m/m_z)$ and κ is an average value of the Ginzburg Landau parameter, $m = (m_x m_y m_z)^{1/3}$, and $\varepsilon = m_x/m_z$. The self-energy of a fluxoid is found to be

$$4\pi F_1 = \frac{\phi_0 H_c}{\sqrt{2}\,\tilde{\kappa}} \left(\ln \tilde{\kappa} + 0.497\right) . \qquad (16)$$

Putting this into equation (2-12) gives

$$H_{c1a} = \frac{H_c/\sqrt{2}\,\tilde{\kappa}\ (\ln\tilde{\kappa} + 0.497)}{\dfrac{\sin\theta_a \sin\theta_B}{1-L} + \dfrac{\cos\theta_a \cos\theta_B}{1-N}} \quad . \tag{17}$$

Minimizing equation (2-17) with respect to θ_B gives the condition for θ_B,

$$(\ln\tilde{\kappa} + 0.497)\left(\frac{\sin\theta_a}{(1-L)\sin\theta_B} - \frac{\varepsilon\cos\theta_a}{(1-N)\cos\theta_B}\right) = \left(\frac{\sin\theta_a \sin\theta_B}{1-L} + \frac{\cos\theta_a \cos\theta_B}{1-N}\right)(1-\varepsilon) \quad . \tag{18}$$

This equation must be solved numerically for each fixed angle of the applied field. In their calculation, Klemm and Clem find only the internal lower critical field. In a later paper, Klemm[7] transforms the internal critical field to the applied critical field using demagnetization factors. These calculations of Klemm are equivalent to our much simpler and more transparent calculation.

The directions of H_a, H_i, and B relative to the crystal axes of a sample are drawn in Fig.II.1. Fig.II.2a shows H_{c1a} plotted against θ_a for a spherical sample with κ=9, for two anisotropies ε=0.119 and ε=0.01. The demagnetization factors for a sphere are L=M=N=1/3, so Fig.II.2a is the same as a plot for the internal critical field. For a mildly anisotropic superconductor (ε=0.119) the curve is continuous, but there is a break in the curve for a very anisotropic superconductor. Changing the parameter κ has little effect on the shape of the curve. A plot of θ_B against θ_a is shown in Fig.II.2b. For ε=0.119 the curve is continuous, but shows that the initial fluxoid is not parallel to the internal field. If it were, then θ_B would equal θ_i, as in the isotropic case. The curve for ε=0.01 is

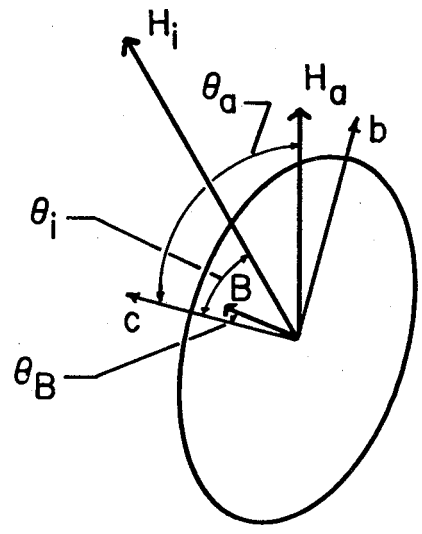

Fig.II.1- Sketch showing definitions of the angles θ_a, θ_i, and θ_B.

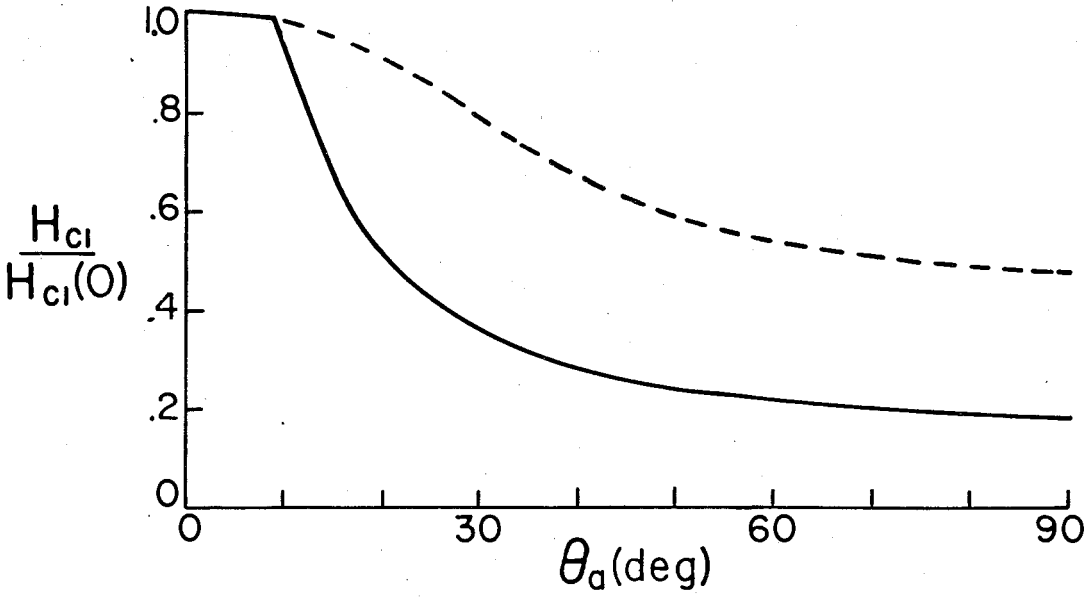

Fig.II.2a- H_{c1} vs θ_a using Klemm and Clem's theory[1] for spherical samples with $\kappa_\perp = 9$ for $\varepsilon = 0.01$ (solid) and $\varepsilon = 0.119$ (dashed).

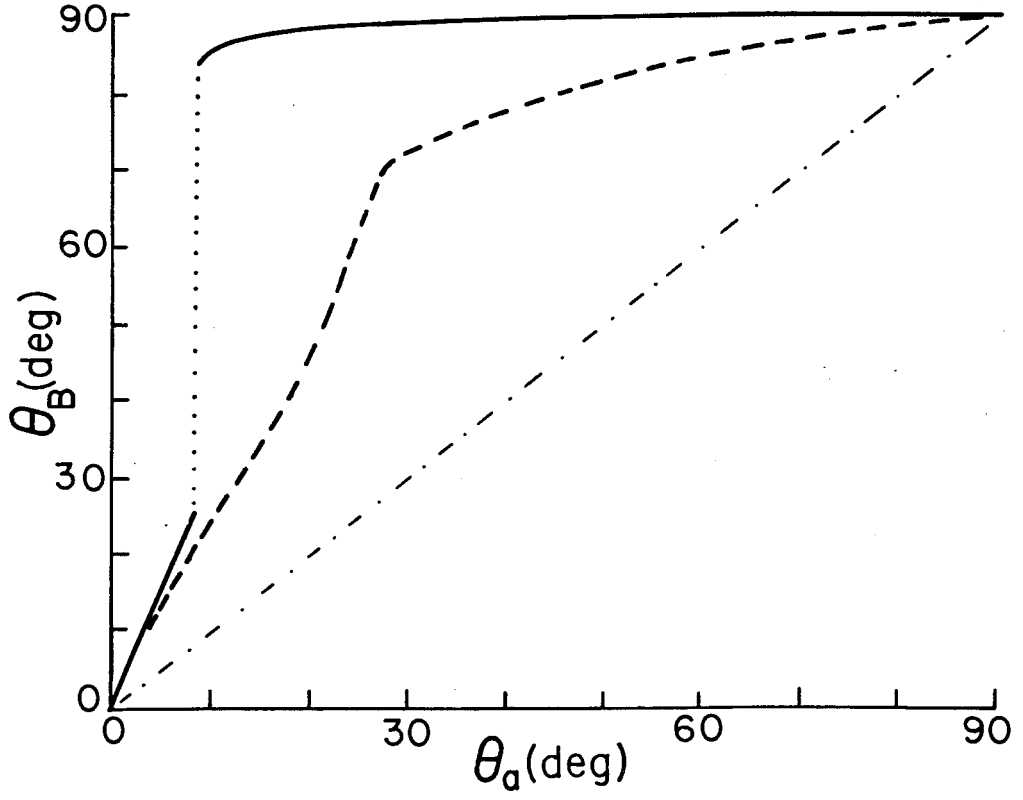

Fig.II.2b- θ_B vs θ_a for the two cases in Fig.II.2a. The dot and dash line shows the curve $\theta_B = \theta_i$.

discontinuous. There is a range of angles θ_B which give directions in which the initial fluxiod will never lie. That is, this range of angles is not allowed. This discontinuity in θ_B marks the position of the break in H_{cla}.

The effects of demagnetization are shown in Fig.II.3, for the case ϵ=0.01. Here H_{cla} vs θ_a is shown for an oblate spheroid with a ratio of the axes of c/a=0.1. Since B=0 at H_{c1}, χ=-1/4π and the internal field is given by

$$H_{ix} = \frac{H_{ax}}{1-L} = 1.075\ H_{ax}$$

$$H_{iz} = \frac{H_{az}}{1-N} = 7.184\ H_{az} \qquad (19)$$

The magnitudes of H_{cla} near the θ=0 direction for the oblate spheroid are much reduced compared to the values for the sphere because the demagnetizing effects are large in this direction. At the same time, the position of features in H_{cla} move from smaller angles for the sphere to larger angles for the spheroid.

It is the appearance of the discontinuity in θ_B vs θ_i, which is reflected in the break of H_{cli} vs θ_i, that triggered the present research. Up to now, these unusual features have never been observed experimentally.

Flux Entry

The theory, so far, has considered only an ideal type II superconductor, for which flux begins entering the bulk of the superconductor at H_{c1}. In a real superconductor there may be effects which

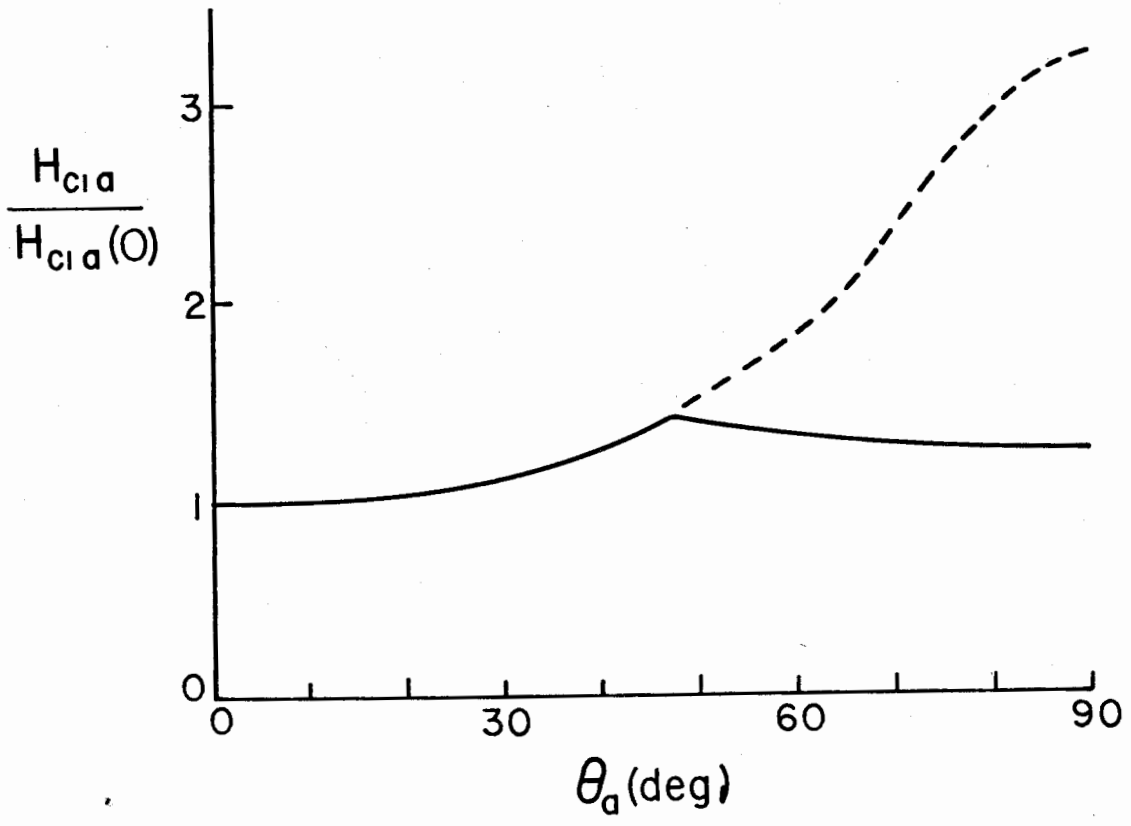

Fig.II.3- H_{c1} vs θ_a using Klemm and Clem's theory[1] for oblate spheroidal samples with ratio of axes c/a=0.1, with $\kappa_\perp$=9 for ε=0.01 (solid) and ε=0.119 (dashed).

delay the entry of flux. A surface barrier to flux entry can exist, for an applied field parallel to the surface of a superconductor, when a fluxoid sees its image in the flat surface.[4] This will delay flux entry to a field H_{en} which is larger than H_{c1}. A roughened or scratched surface will minimize the surface barrier. Another possible cause of delayed flux entry is flux pinning. As the flux begins to enter a superconductor, the fluxoids can become pinned on defects in the superconductor. A field larger than H_{c1} is needed to move the fluxoids past the pinning centers. This situation is described by the theory of the Critical State.[3,10,11] This theory assumes that any emf, however small, will induce a transport supercurrent which is equal in magnitude to the critical current of the superconductor. When flux first crosses the surface of the superconductor this irreversible transport current is induced in a layer at the surface which shields against further flux entry. As the externally applied field is increased the layer containing the shielding current grows.

The solid line in Fig.II.4 shows a magnetization curve for an ideal type II superconductor. At H_{c1} there is little resistance to flux entry and the magnetization decreases sharply. The magnetization curve for an ideal superconductor is reversible. Effects which delay flux entry will cause an irreversible magnetization curve as shown by the dashed line in Fig.II.4. Magnetization measurements of a superconductor will give the field H_{en} where the flux first enters a superconductor. This entry field may be larger than the lower critical field.

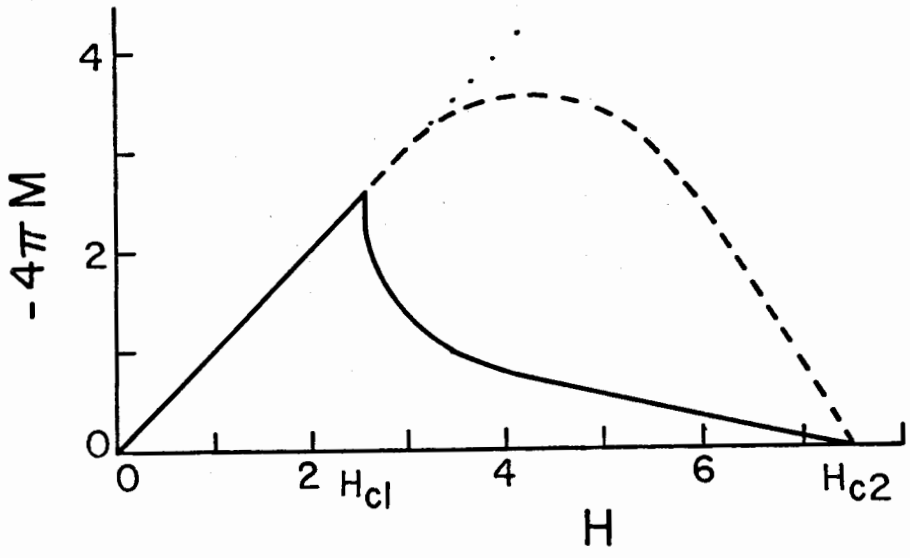

Fig.II.4- Ideal magnetization curve (solid) and irreversible magnetization curve (dashed) for type II superconductors. Only the initial branch of the irreversible curve is shown.

III. SQUID Magnetometer

The magnetometer has the capability to measure changes in either the dc or the ac magnetization of a sample. It can be operated with a fixed applied field where the temperature of a sample is varied or the temperature can be held constant and the applied field varied.

An overall view of the magnetometer is shown in Fig.III.1. The sample holder sits in an evacuated tube to insulate the sample from the liquid helium bath. An O-ring seal and an in-line valve at the top of the magnetometer allow the sample holder to be removed without letting air into the magnetometer. Thin walled stainless steel tubes run from room temperature into the liquid helium to minimize heat conduction into the bath. A vacuum tight joint between the pyrex tube and the copper tube was made using Epibond 1266 epoxy mixed with an equal amount, by weight, of powdered pyrex glass. The construction and operation of each part of the magnetometer is discussed in this chapter.

SQUID

The SQUID unit is made by SHE,[12] model 330. The SQUID probe itself is contained in a superconducting case and located near the bottom of the magnetometer (see Fig.III.1). An input signal is brought to the SQUID probe using superconducting niobium wire which makes superconducting connection with the SQUID probe using niobium screws. The SQUID functions as a microammeter with a maximum sensitivity of 0.0952 μA input giving 1.98 V output. This is about 0.05 μA/V.
0,0481

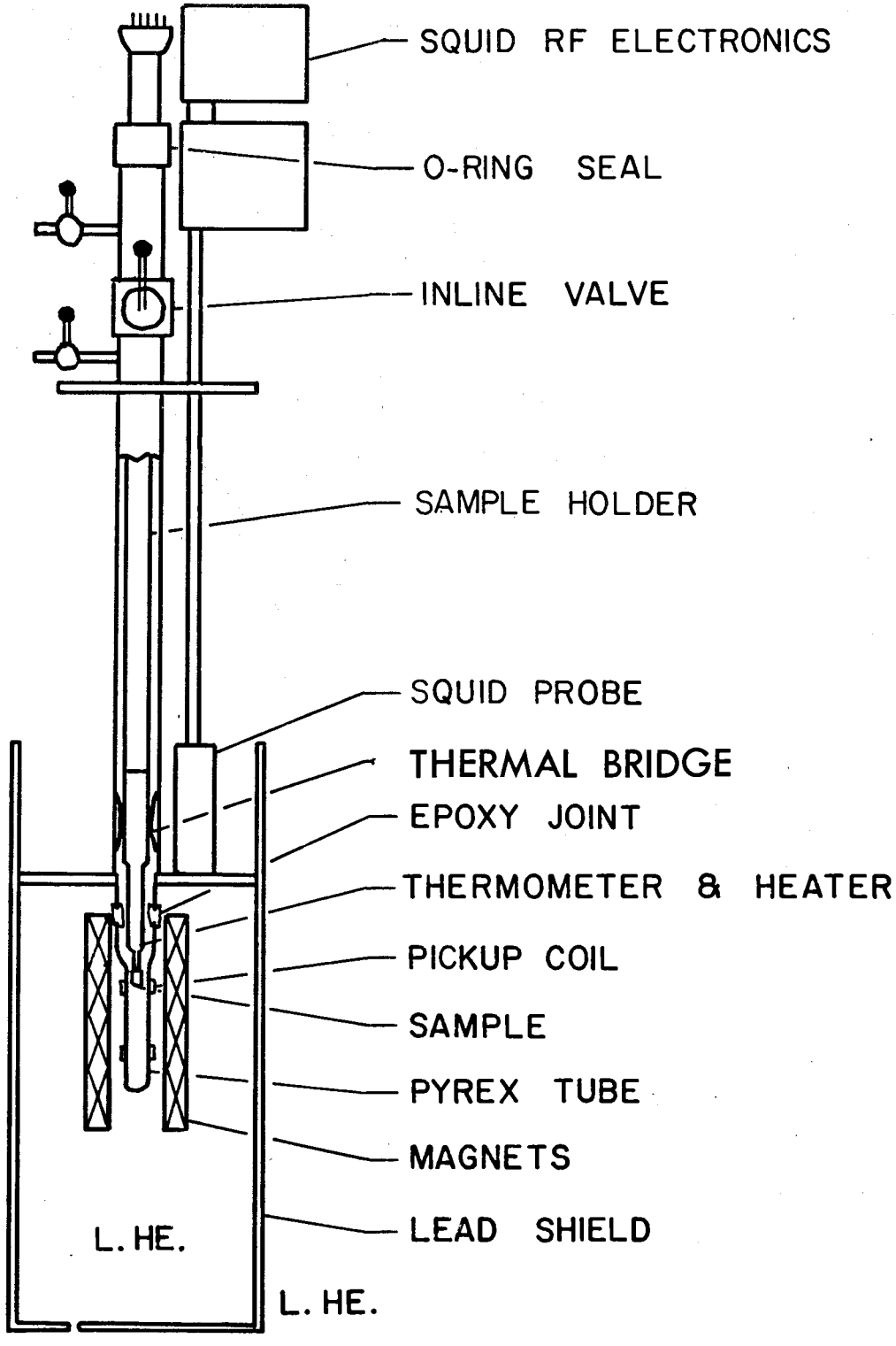

Fig.III.1- Diagram showing the construction of the SQUID magnetometer. The lower portion is shown in cross-section.

Flux Transformer

A sample is placed at the center of one of two pickup coils as shown in Fig.III.2. The coaxial pickup coils are identical but wound in opposition from a single superconducting wire. A complete superconducting path is made by connecting the pickup coils to a signal coil which is inside the SQUID. Connecting leads are tightly twisted to minimize their self inductance. A change in magnetization of the sample will induce a current in the top pickup coil due to their mutual inductance. This current then couples the change in magnetization to the SQUID through the signal coil. Since the flux transformer is superconducting, it works even for dc signals. If the two pickup coils are in perfect balance a changing uniform field will not induce a current in the flux transformer.

Since the total flux linked by a superconducting loop must remain constant, the total flux linked by the flux transformer will remain constant. Let ϕ_{ext} be the flux linked by one loop of the top pickup coil due to a change in magnetization of the sample. The flux linked by the pickup coil will be $N\phi_{ext}$, where N is the number of turns on the pickup coil. In order to keep the total flux constant a supercurrent J is induced in the superconductor. The flux linked by the flux transformer due to J is just JL, where L is the total self inductance of the flux transformer. If L_{sg}, L_{pu}, and L_{ld} are the inductances of the signal coil, one pickup coil, and the twisted leads respectively, then

$$L = L_{sg} + L_{ld} + 2L_{pu} \quad . \tag{1}$$

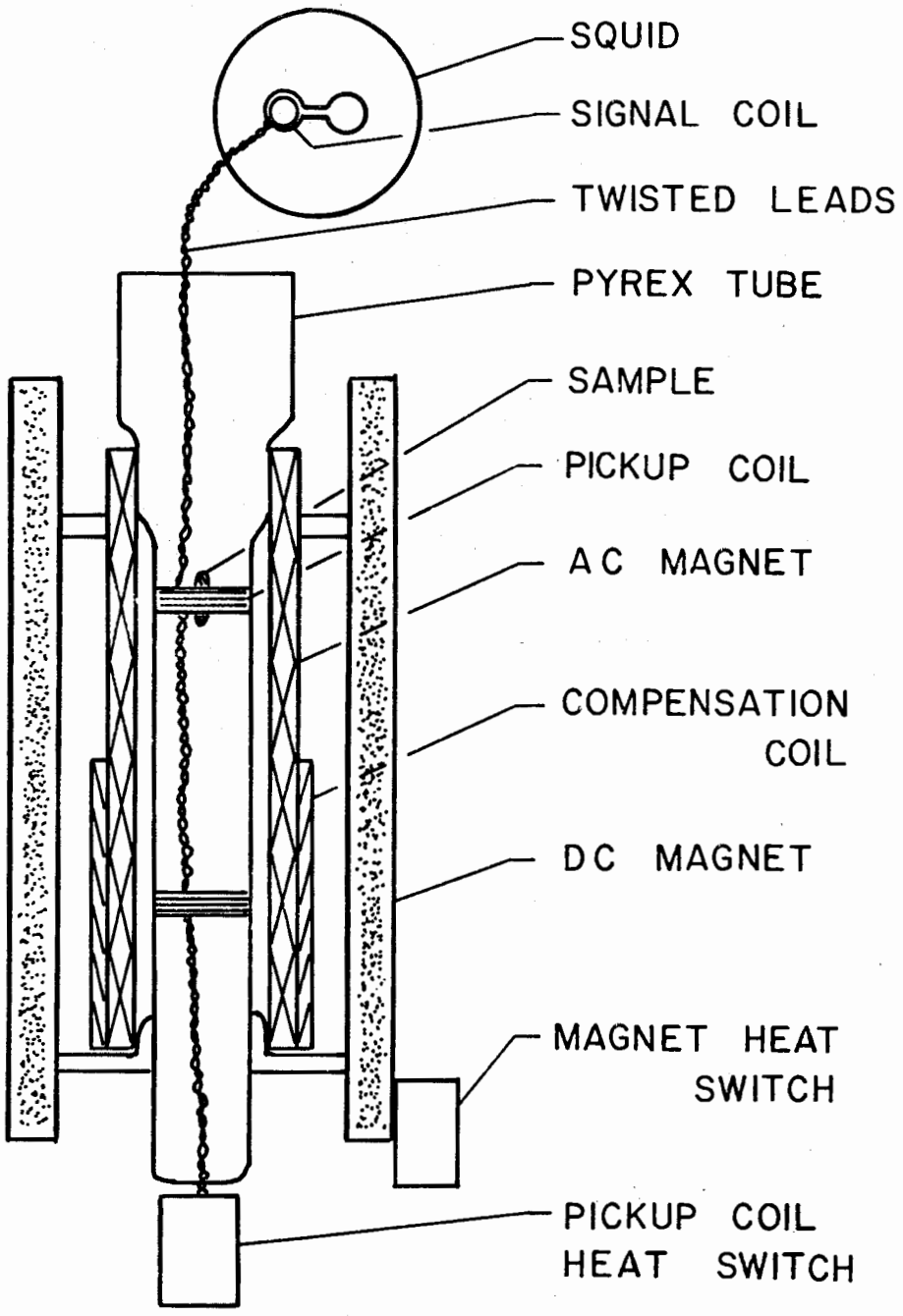

Fig.III.2- Diagram showing the flux transformer and the magnets.

Since the flux linked due to J must balance the flux linked due to the sample,

$$N\phi_{ext} = -(L_{sg} + L_{ld} + 2L_{pu})J \quad . \tag{2}$$

The flux linked by the SQUID due to the current J is

$$\phi_{SQ} = M_{sg} J \quad , \tag{3}$$

where M_{sg} is the mutual inductance of the SQUID and the signal coil. Combining the last two equations gives the basic equation for a flux transformer[13]

$$\phi_{SQ} = \frac{-M_{sg} N}{(L_{sg} + L_{ld} + 2L_{pu})} \phi_{ext} \quad . \tag{4}$$

In designing a flux transformer one usually attempts to maximize the flux transfered to the SQUID. In our comercial SQUID, M_{sg} and L_{sg} are part of the SQUID probe and are fixed. The inductance of the twisted leads is very small (about 0.3 μH per meter[13]) and will be neglected. Maximizing ϕ_{SQ} is a matter of making N as large as possible while keeping L_{pu} as small as possible. Since L_{pu} is proportional to N^2, the condition for maximizing ϕ_{SQ} is $2L_{pu}=L_{sg}$. N and ϕ_{ext} are maximized by making the pickup coil as small as possible (with it still being in the liquid helium bath). The pickup coils used were made of 0.003 inch diameter niobium wire. Each was a seven turn single layered coil with L_{pu}=0.8 μH. The signal coil has L_{sg}=1.8 μH, which is about the same as $2L_{pu}$.

The heat switch (Fig.III.2) does not affect the normal operation of the flux transformer. It is operated when a large dc field is being applied, and keeps the current in the flux transformer equal to zero. A

large current could put the SQUID out of its range of linear opperation and could even damage the Josephson junction. The heat switch is constructed by placing a section of the superconducting leads against a 10KΩ metal film resistor and encasing these with epoxy. Applying a few milliamps to the resistor heats the flux transformer wire above its critical temperature. Any supercurrent in the flux transformer will decay rapidly.

Magnets

A magnetic field can be applied by one of two solenoids (Fig.III.2). The dc magnet is used to apply a constant magnetic field in the persistant mode. The ac magnet is used to apply a changing (or ramped) dc field or an ac field. Both coils are wound from superconducting wire with copper cladding (Supercon,[14] T48B). The ends of the dc magnet's windings are spot welded together to form a complete superconducting path. A section of the wire can be driven normal using a heat switch, similar to the heat switch used with the flux transformer. A current is induced in the magnet by applying a voltage across the normal section. When the heat switch is turned off, there is a closed superconducting path and the current is maintained without an externally applied voltage. Since the flux linked by a superconducting loop must remain constant, the dc magnet gives a very stable field.

The ac magnet does not operate in the persistant mode. Any electrical noise, from the current supply or picked up in the leads, will affect the applied field. In particular, even a small amount of rf noise will interfere with the operation of the SQUID. Rf noise is filtered out using

low pass R-C filters placed just above the ac magnet and compensation coil. Ideally a ramped or ac field, applied in the absence of a sample, would not induce a signal in the flux transformer. In practice the pickup coils are not quite identical and the field is not quite uniform. There will be a small "out of balance" signal. This out of balance signal is cancelled using a small compensation coil placed around the lower pickup coil (Fig.III.2). In the case of an applied ac field, both the amplitude and phase of the current in the compensation coil must be adjusted to give a null signal. This was accomplished using an SHE impedance bridge, model RBU.

The magnets and pickup coils are encased in a closed-bottom, superconducting , lead cylinder. This is an effective shield against magnetic noise from the environment.

The magnetic field produced by the dc coil in free space was found by using the standard formula for a solenoid of infinite length, then applying a correction for finite length from a table (Lorrain and Corson[15] page 347). This field constant for the dc coil in free space is H/I=1.066 Oe/ma. When the coil is placed inside a superconducting cylinder the field changes. Fig.III.3 shows the situation. Applying Ampere's law twice along the paths shown and noting that the flux through a cross-section of the superconducting cylinder must remain constant, gives

$$H_i = H_o \frac{A_s - A_o}{A_s} \qquad (5)$$

H_i is the field inside the solenoid, H_o is the field inside the solenoid without the superconducting shield, A_s is the cross-sectional area of the shield, and A_o is the cross-sectional area of the solenoid. Applying this

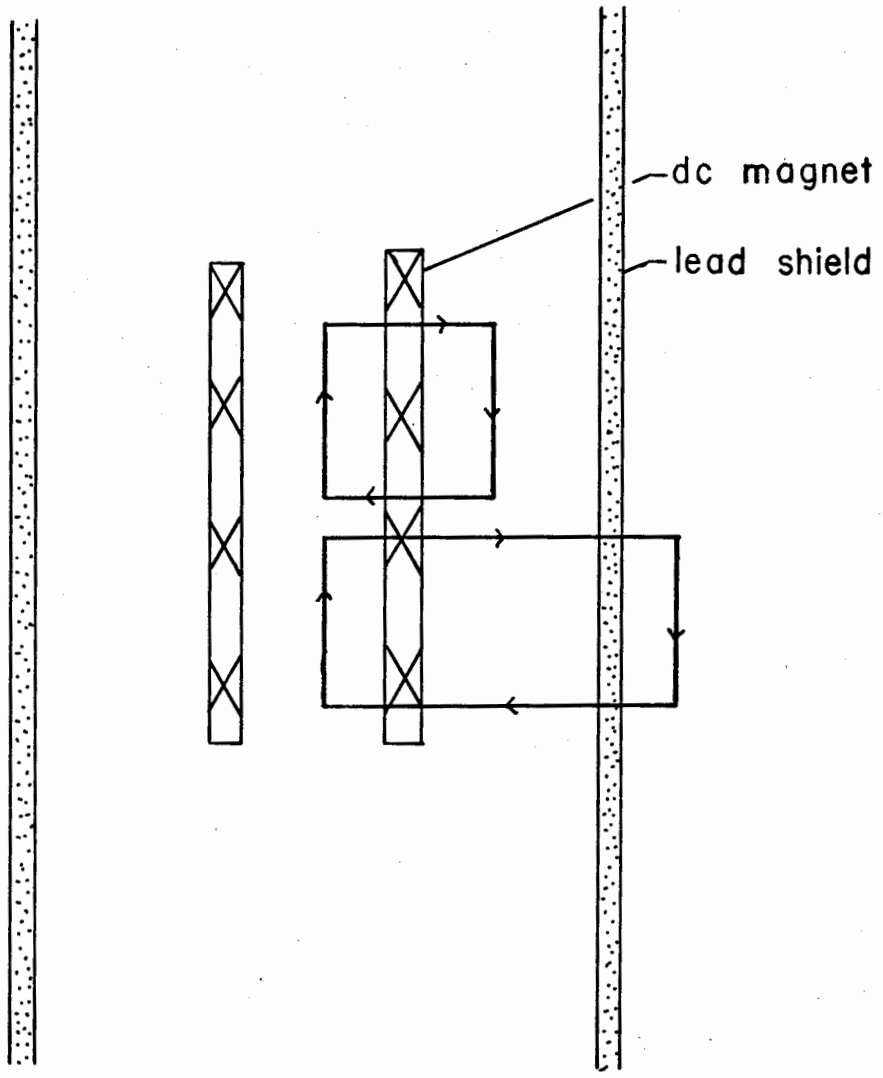

Fig.III.3- Line integrals used for the field calculation.

correction gives for the dc coil, $H_i/I=0.85$ Oe/ma.

This field calibration was checked experimentally in two ways. First by measuring the height of the superconducting to normal transition of a sample with known volume and demagnetization. Knowing the characteristics of the flux transformer, the flux linked from the sample to the pickup coil,[16] and the SQUID sensitivity, the value of the applied field can be deduced. Two measurements gave values of $H/I=(0.82\pm0.05)$Oe/ma and $H/I=(0.84\pm0.05)$Oe/ma. This is in good agreement with the calculation. The other experimental check was made by measuring the temperature dependence of the critical field of a lead sample and comparing this with the literature result. This gave a field calibration of $H/I=(0.86\pm0.04)$Oe/ma. Again there is good agreement.

The field calibration of the ac coil was made by comparing transition heights, produced by the dc and ac coils. The field constant for the ac coil is $H/I=(0.49\pm0.04)$Oe/ma.

Sample Holder

The sample holder positions the sample inside the pickup coil as shown in Fig.III.1. The thermal bridge is made of copper and makes mechanical contact with the sample holder. This centers and holds the lower end of the sample holder. The thermal bridge also puts the sample holder in contact with the 4.2 K liquid helium bath.

Fig.III.4 shows the lower end of the sample holder. It is the thermal anchor section of the sample holder which makes contact with the thermal bridge. The function of the radiation shield and the thermal anchor is to prevent heat from the top of the sample holder from warming the thermometer

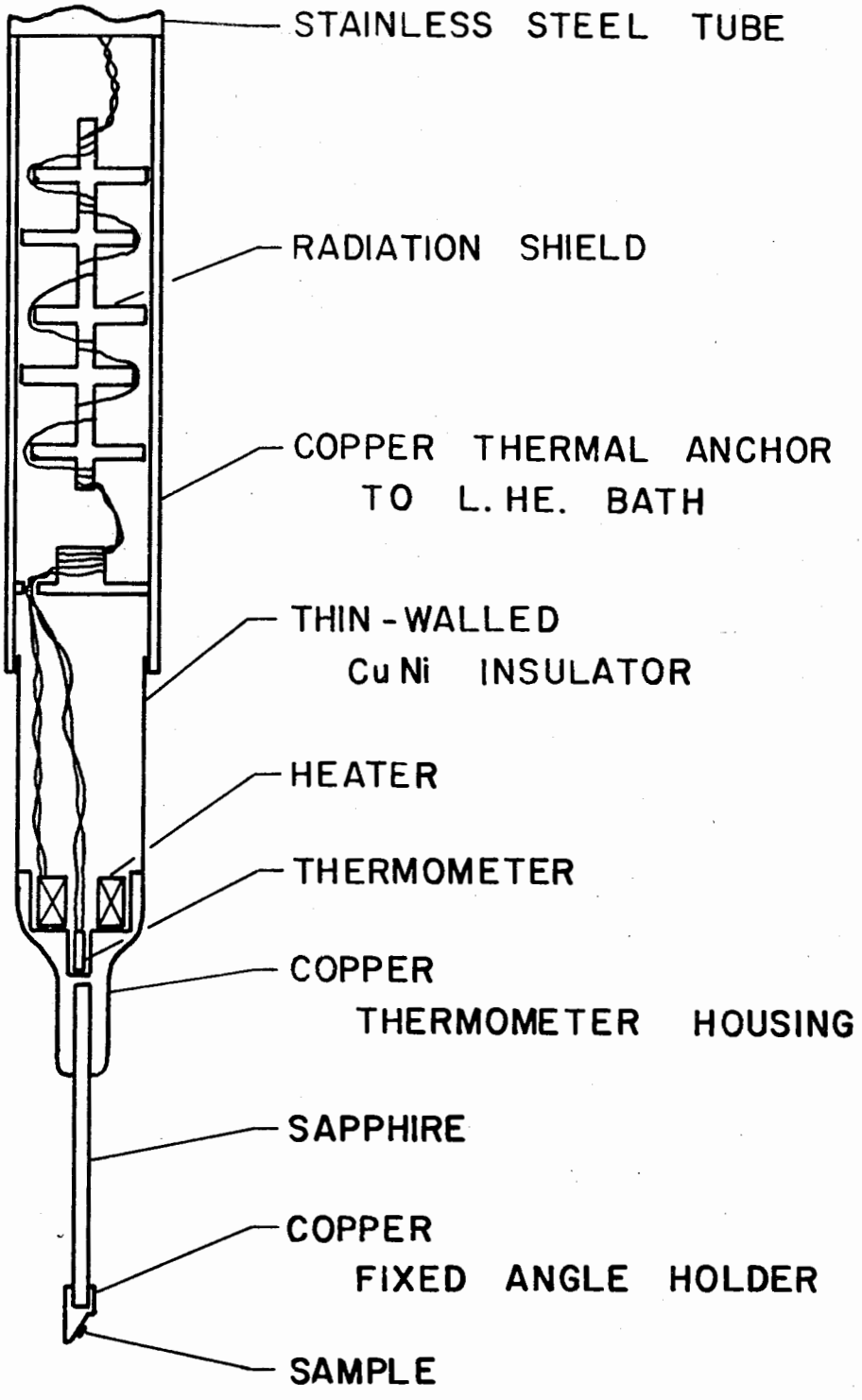

Fig.III.4- Details of the lower portion of the sample holder.

or the sample itself. Heat conducted down the electrical leads and the stainless steel tube is absorbed by the thermal anchor. The radiation shield consists of a number of metal discs held at 4.2 K. It absorbs the 300 K radiation which comes from the top of the sample holder. The entire sample holder is evacuated. The sample is held on the bottom of the sample holder (Fig.III.4). In order to minimize the magnetic background seen by the magnetometer, the thermometer and heater must be kept some distance away from the pickup coil. Thermal contact between the heater and thermometer is made by a sapphire rod. Sapphire is a good thermal conductor and yet is an electrical insulator. This is of particular importance if there is an ac applied field, since a conductor will give a large magnetic response due to induced eddy currents. The sapphire rod is set into a close-tolerance hole in the copper thermometer housing using Apiezon grease. The H_{c1} measurements reported in this thesis were made with dc applied fields. This allows the use of interchangable copper fixed angle holders at the bottom of the sapphire rod. These fix the angle of the sample relative to the applied field. The copper angles and the samples are also held on with Apiezon grease. The thermometer is a calibrated carbon glass resistance thermometer. The heater is a bifilarly wound coil of manganin wire. A thin-walled cuprous nickel tube connects the thermometer housing to the thermal anchor, to allow only a small thermal conductance between the two. In addition, to minimize thermal conductance, the thermometer and heater leads up to the thermal anchor are thin constantan wire and thin manganin wire, respectively.

Heating the sample is accomplished by applying current to the heater. The sample is cooled by thermal conduction to the thermal anchor, radiation

to the liquid helium bath, and conduction through a small amount of helium exchange gas (let into the vacuum space in which the sample holder sits). For temperatures less than 10 K, the dominant form of cooling is through the exchange gas. Since the thermometer is some distance from the sample, when heating or cooling the sample, there will be a temperature lag between the thermometer and the sample. To minimize this, the temperature should be changed slowly. A typical rate of temperature increase would be about half a degree in five minutes. Even at a constant temperature, the sample will be somewhat cooler than the thermometer. This temperature difference was found to be about 0.05 K by measuring T_c for a lead sample and comparing it to the accepted value. It varied for different amounts of exchange gas. This difference was found to remain constant over a small range of temperatures (about half a degree) by measuring the temperature dependence of H_c for a lead sample.

Magnetization Measurements

This apparatus does not measure absolute magnetization. Rather, it measures changes in magnetization. There are two ways to induce a change in the magnetization of a sample. The temperature can be varied or the applied field can be varied. In order to measure the temperature induced superconducting transition, the sample is first cooled to well below T_c in zero applied field. Then a constant field is applied using the dc magnet in the permanent mode. The temperature is then raised slowly and the SQUID output is recorded. A typical transition is shown in Fig.III.5. At low temperatures the sample is in the Meissner state and its magnetization is $M=-H_i$. At temperatures above T_c, the sample is normal and its magnetization

is practically zero. The transition height is the total change in SQUID output from the Meissner state to the normal state. This is proportional to the internal field in the sample when it was in the Meissner state. In addition to the dc field, an ac field can be applied. In this case, both the in phase and 90° out of phase responses can be recorded. Ac measurements are not reported in this thesis, but this technique is described elsewhere.[17] The other mode of operation of the magnetometer is the field sweep mode. The temperature of the sample is lowered in zero field to below T_c. The temperature is held fixed while a dc field is slowly applied using the ac coils. The balancing current which is in the compensation coil changes at the same rate as the current in the main ac coil. The SQUID output gives the changing magnetization of the sample.

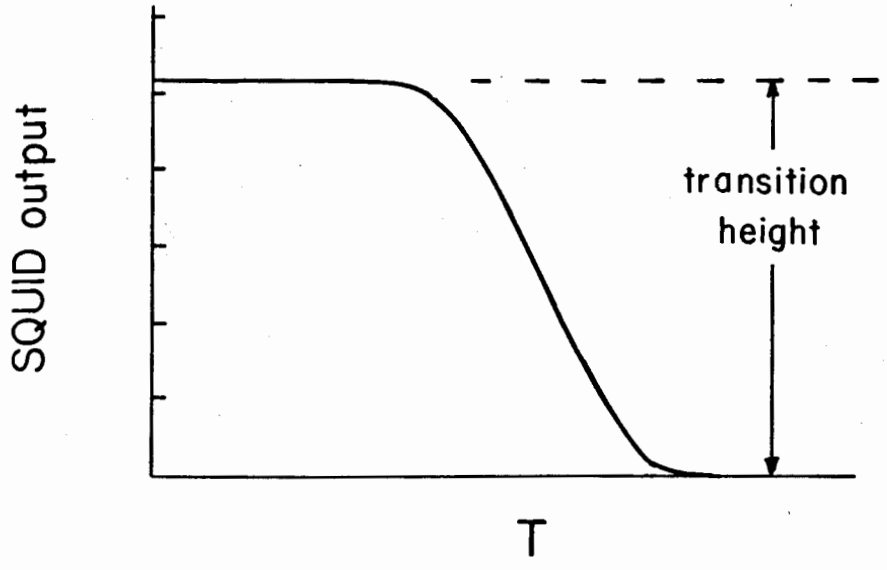

Fig.III.5- A typical temperature induced superconducting transition.

IV. Results - Isotropic Superconductor

Samples

In order to investigate the effects of demagnetization and as a check on the magnetization method for measuring H_{c1} a large κ, isotropic superconductor was first used. Samples were made from a bar of niobium 48 atomic percent titanium. This bar was obtained from Supercon.[14] The Nb48%Ti was annealed, in vacuum, in an induction oven at 1200 C for four hours. A small amount of evaporation of the sample occurred. It was assumed that more titanium was lost than niobium since titanium has the higher vapor pressure. The resulting sample would contain a small amount less than 48% titanium. The exact composition of the sample is not important for our investigation. There are no measurements of H_{c1} for Nb48%Ti in the literature to compare with the results here, but the main interest in measuring H_{c1} for an isotropic superconductor is to investigate the effects of demagnetization. It is important that the sample be uniform and isotropic. Annealing is necessary to obtain this. Samples in the shape of oblate spheroids were made from the annealed Nb48%Ti using a lathe, a small file, and emery paper. Their surfaces were smoothed by etching in a fresh mixture of two parts H_2SO_4, one part HF, and one part 30% hydrogen peroxide for five minutes. The surfaces were smooth but not shiny.

Demagnetization

The height of the magnetic transition from the Meissner state to normal can be used to find the demagnetization of the sample. Since the magnetization is proportional to the internal field, the demagnetizing factors can be found by measuring the transition heights along the axes of symmetry of the sample. These measurements were made using two Nb48%Ti ellipsoids of different shapes.

For an ellipsoid with the applied field along its z-axis, as shown in Fig.IV.1a, the exact flux linked to the pickup loop can be calculated. The field distribution outside an ellipsoid in a uniform applied field can be found using ellipsoidal coordinates in the same way as demagnetizing factors are found as mentioned in Chapter II. The integral of field over the area of the pickup loop can be done analytically. These calculations have been published elsewhere.[16] For an oblate spheroid of height 2c in the z direction and diameter 2b in the x-y plane in a pickup loop of radius ρ, the flux linked by the pickup loop is

$$\phi = \frac{6\pi m}{a}\left\{\frac{-1}{2}\left[\left(\frac{\rho}{a}\right)^2-1\right]\left(\arctan\left(\left[\left(\frac{\rho}{a}\right)^2-1\right]^{-1/2}\right) - \left[\left(\frac{\rho}{a}\right)^2-1\right]^{-1/2}\right.\right.$$
$$\left.\left. + \frac{1}{2}\arctan\left(\left[\left(\frac{\rho}{a}\right)^2-1\right]^{1/2}\right) - \frac{\pi}{4}\right\} \quad , \qquad (1)$$

where $a=b/\cosh\eta$, $\eta=\operatorname{arcsinh}(b/c)$, and m is the magnetic dipole moment $m=MV$ where M is the magnetization and V is the sample volume. For other angles between the c axis and the applied field the flux integral can not be done analytically. For a sample which is much smaller than the pickup loop the flux linked approaches the form of the flux linked for a dipole (spherical sample) which is

$$\phi_{dipole} = \frac{2\pi m}{\rho} \quad . \qquad (2)$$

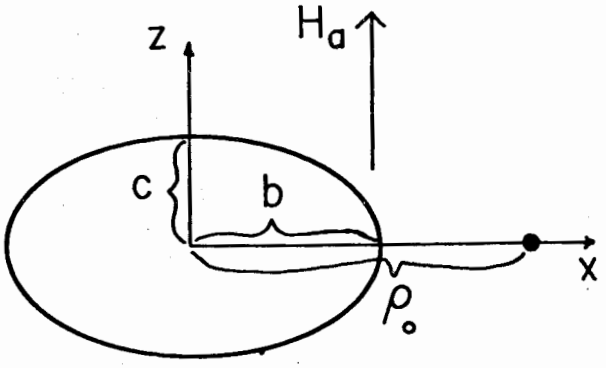

Fig.IV.1a- An oblate ellipsoid in the pickup loop with the applied field parallel to the c-axis.

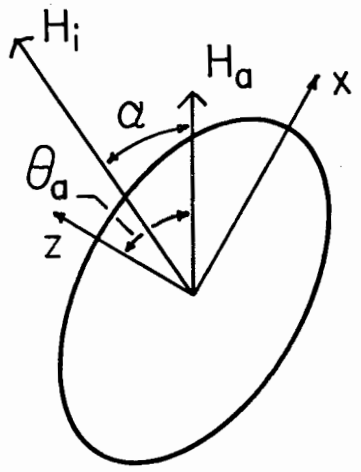

Fig.IV.1b- The sample rotated an angle θ_a with respect to the applied field.

The difference between the exact flux calculation and the dipole approximation will be greatest when the applied field is along the c axis, since this is when the sample fills the greatest area in the plane of the pickup loop. If the dipole approximation is good when the field is along the c axis, it will be good for all directions.

Using the dipole approximation the ratio of the transition height S(0) for a field along the c axis to the transition height S(90) for a field along the b axis is

$$\frac{S(0)}{S(90)} = \frac{\phi(0)}{\phi(90)} = \frac{2\pi M(0) V/\rho}{2\pi M(90) V/\rho} = \frac{M(0)}{M(90)} = \frac{1/1-N}{1/1-L} \quad , \qquad (3)$$

using $M=-H_i$ and equation (2-5). Using the identity L+M+N=1 for the demagnetizing factors and using the measured transition heights, the demagnetizing factors for the two samples were found. These results along with the calculated demagnetizing factors, using equations (2-6), are given in Table IV.1. The dipole approximation was good for the smaller more spherical sample, Nb48%Ti#1, and the measured transition heights were used for S in equation (4-3). But for the larger flatter sample, whose radius was about 1/4 the radius of the pickup coil radius, the exact flux linked given by equation (4-1) is 2% larger than that of the dipole equation (4-2). Therefore the measured transition height when the field was along the c axis was reduced by 2% to find S(0). It was assumed the dipole approximation was still good when the field was along the b axis. The calculated and measured values of L and M in Table IV.1 are in good agreement.

As a check on calculations of internal field for intermediate angles between the applied field and the c axis, the transition heights were also

measured over a range of angles. This situation is shown in Fig.IV.1b. The internal field and the magnetization are no longer in the same direction as the applied field. This situation can be treated exactly in the case of a dipole. If the angle between the magnetic moment of the dipole and the axis of the pickup loop is α the flux linked by the pickup loop is

$$\phi(\alpha) = \phi_{dipole} \cos\alpha = \frac{2\pi m}{\rho} \cos\alpha \quad . \tag{4}$$

The angle α is the difference between the angle of the applied field θ_a and the angle of the internal field θ_i. Using the demagnetization formula from Chapter II,

$$\theta_i = \arctan\left[\frac{1-N}{1-L} \tan\theta_a\right] \quad . \tag{5}$$

Since the dipole moment is proportional to the internal field H_i, the transition height S is proportional to H_i,

$$S(\theta_a) = K H_i \cos\alpha \quad . \tag{6}$$

K is a normalization constant and H_i can be found from

$$H_i = H_a\left[\left(\frac{\sin\theta_a}{1-L}\right)^2 + \left(\frac{\cos\theta_a}{1-N}\right)^2\right]^{1/2} \quad . \tag{7}$$

Measured $S(\theta_a)$ for Nb48%Ti#2 are shown in Fig.IV.2 along with the curve calculated from equation (4-6). There is fairly good agreement between the measurements and the calculations. The measurements fall below the calculation as α gets larger. This suggests that the correction for a dipole, cos α, does not quite hold for the sample Nb48%Ti#2.

This section shows that demagnetizing effects can be taken into account quantitatively.

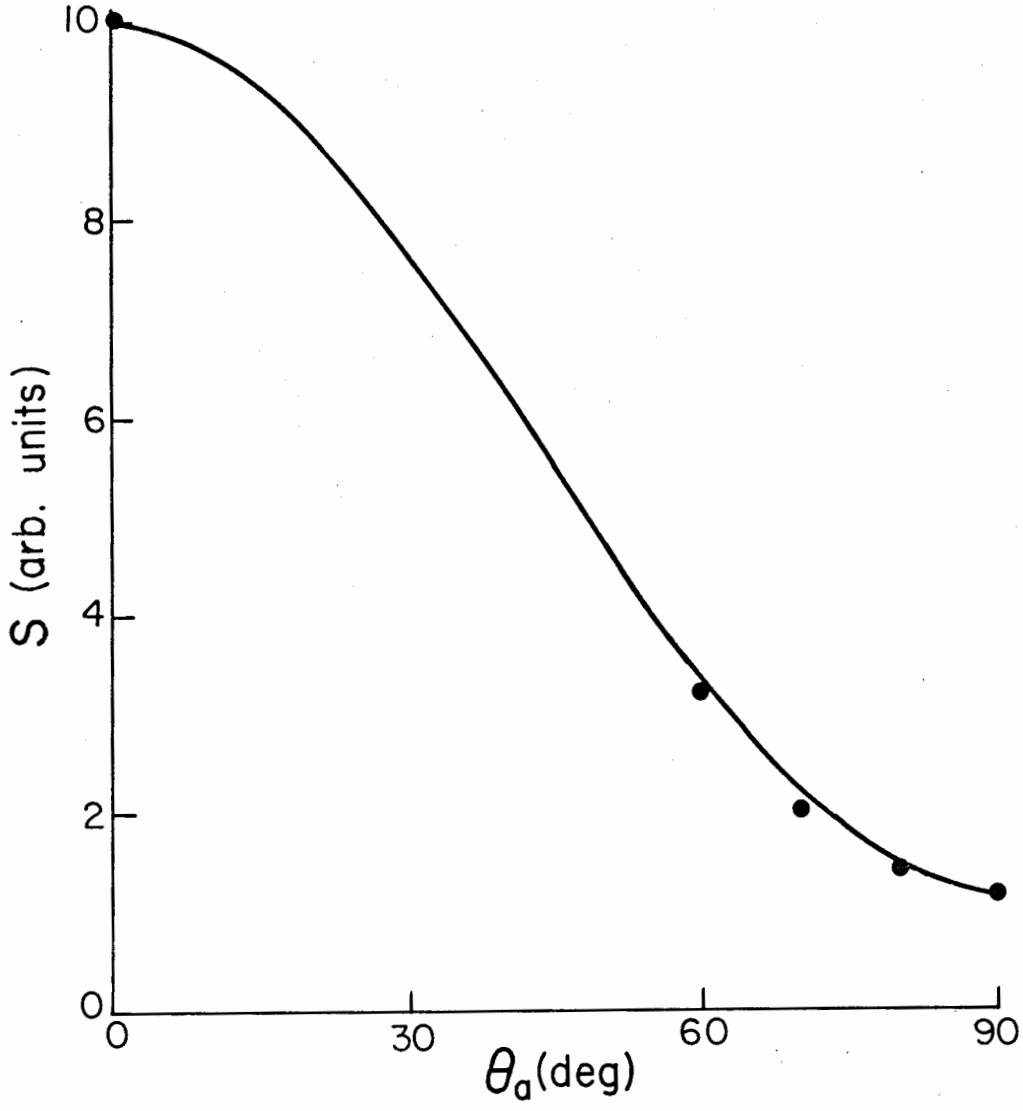

Fig.IV.2- Measured (dots) and calculated transition heights plotted against the applied field for Nb48%Ti#2.

Measurement of the Entry Field

The temperature induced magnetic transition is used to find H_{en}. Fig.IV.3 shows a typical set of transitions for different applied fields, with the sample held at a fixed angle. In each case the sample is cooled from above the transition temperature T_c to well below T_c in zero applied field. Then a constant field is applied using the dc magnet in the persistent mode. The sample temperature is raised slowly and the magnetization is recorded. At low temperatures the sample is in the Meissner state and the curves all follow the same path. As the temperature rises, the curve coresponding to the highest applied field breaks away from the other curves. This point is where the first flux entry occurs. It gives the temperature $T(H_{en})$ for which that particular applied field is H_{en}. The dashed line shows the irreversible curve obtained upon cooling the sample from above T_c with an applied field of 3.4 Oe.

Fig.IV.4 shows a plot of H_{en} vs T using the values of $T(H_{en})$ determined from Fig.IV.3. Theory predicts that the curve H_{c1} vs T should be linear near T_c. The slope dH_{en}/dT is found from graphs like Fig.IV.4 for various θ_a. Results for the two samples, Nb48%Ti#1 and #2, are given in Table IV.2. The slopes of the internal field are found from the measured applied field values using equation (4-7). The four values for the internal field dH_{eni}/dT are in good agreement with each other. This shows that the only effect that the shape of these samples has on the value of H_{en} is due to demagnetization.

H_{en} was measured for some intermediate angles using Nb48%Ti#2.

Table IV.1

The semiaxes of the two Nb48%Ti samples along with the calculated and measured demagnetization factors.

			calculated		measured	
sample	b(mm)	c(mm)	L	N	L	N
#1	0.47	0.245	0.242	0.516	0.239	0.522
#2	0.79	0.064	0.0576	0.885	0.0576	0.887

Table IV.2

The measured $H_{en}(0)$ and $H_{en}(90)$ for the Nb48%Ti samples along with the calculated internal fields, $H_{eni}(0)$ and H_{eni}.

sample	$dH_{en}(0)/dT$	$dH_{en}(90)/dT$	$dH_{eni}(0)/dT$	$dH_{eni}(90)/dT$
#1	-34±4(Oe/K)	-56±5(Oe/K)	-71±8(Oe/K)	-74±7(Oe/K)
#2	-8.2±0.4	-68±5	-72± 5	-72±6

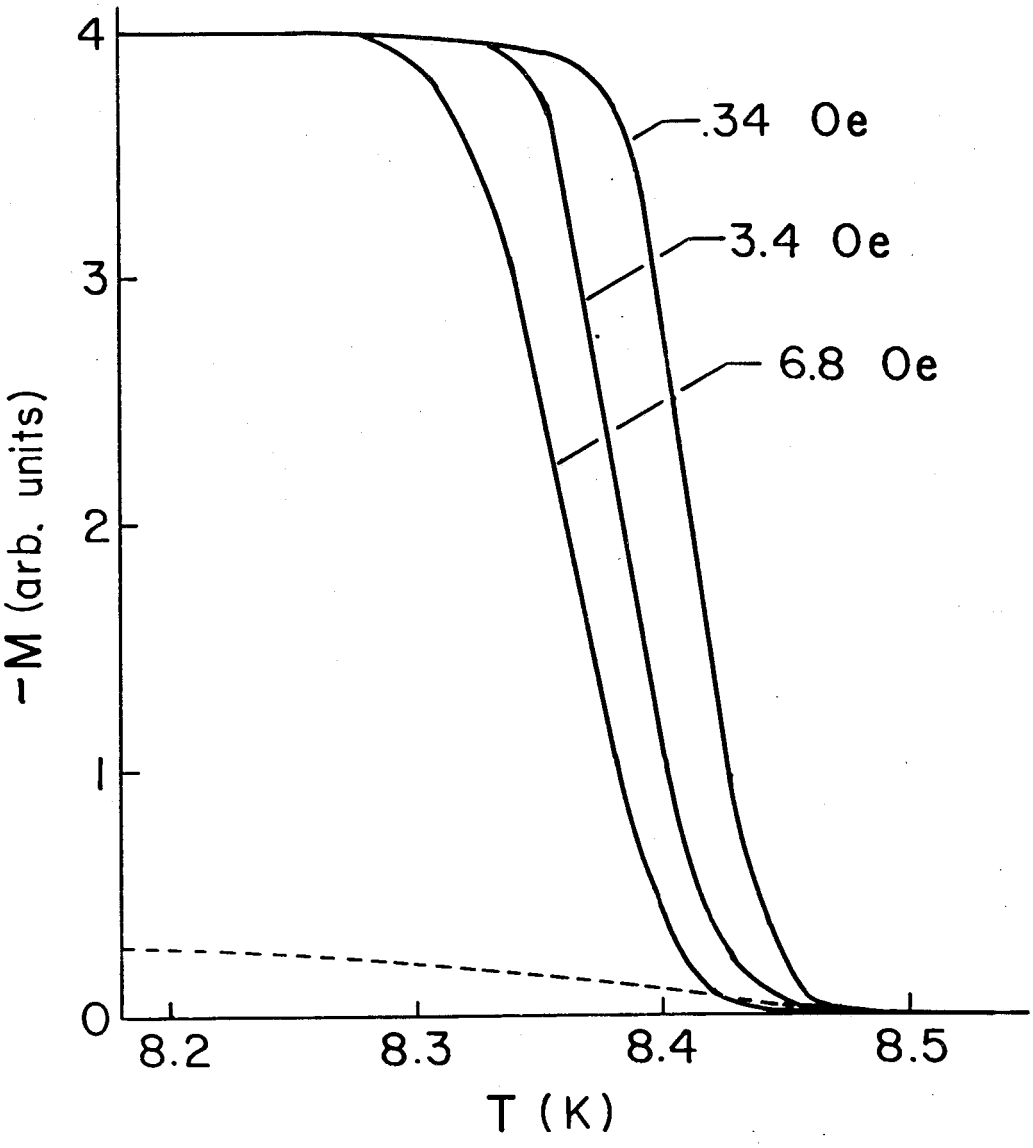

Fig.IV.3- Temperature induced magnetic transitions for Nb48%Ti#2 with θ_a=90. The cooling curve (dashed) is shown for an applied field of 3.4 Oe.

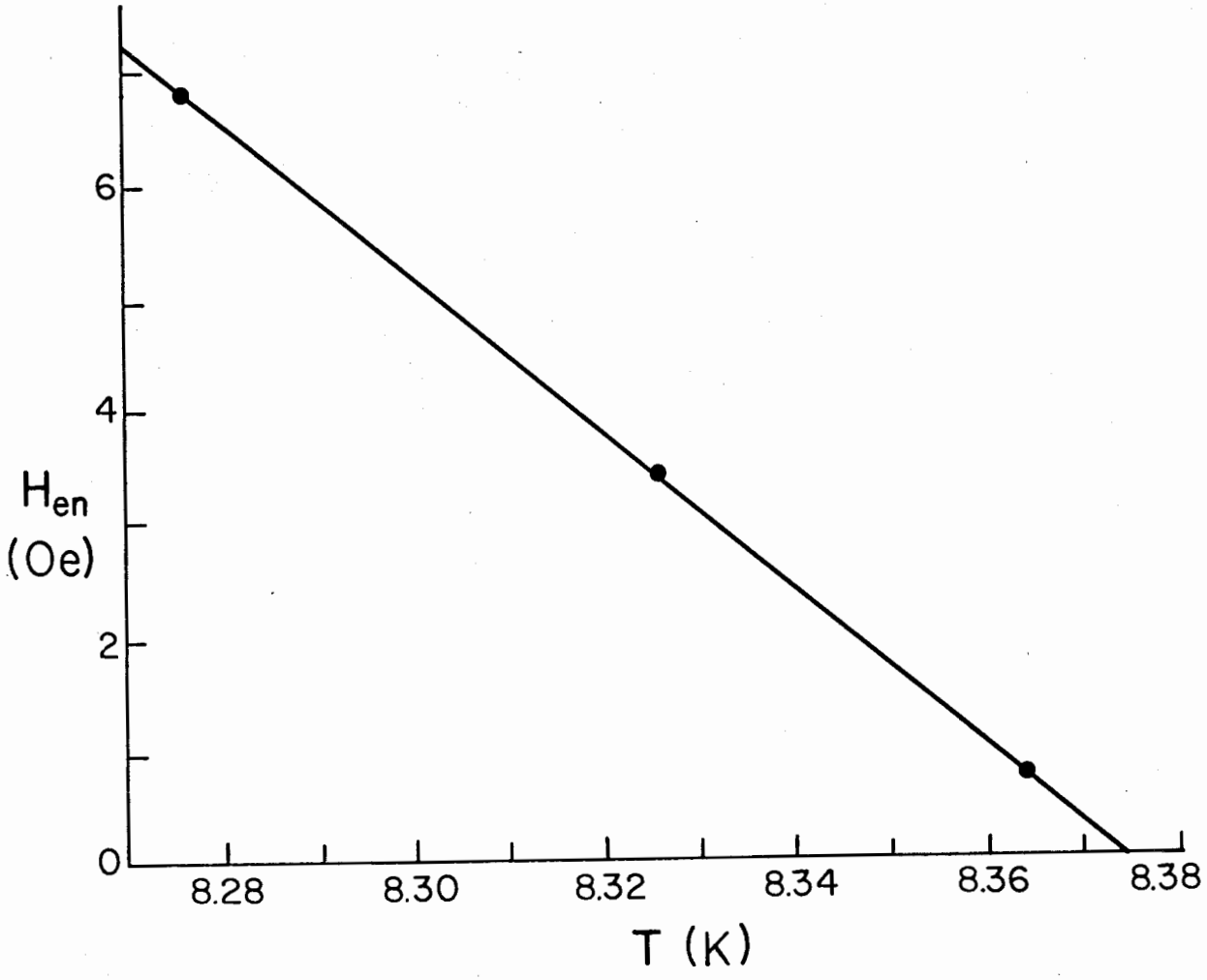

Fig.IV.4- A plot of experimentally determined H_{en} vs T for Nb48%Ti#2 for θ_a=90.

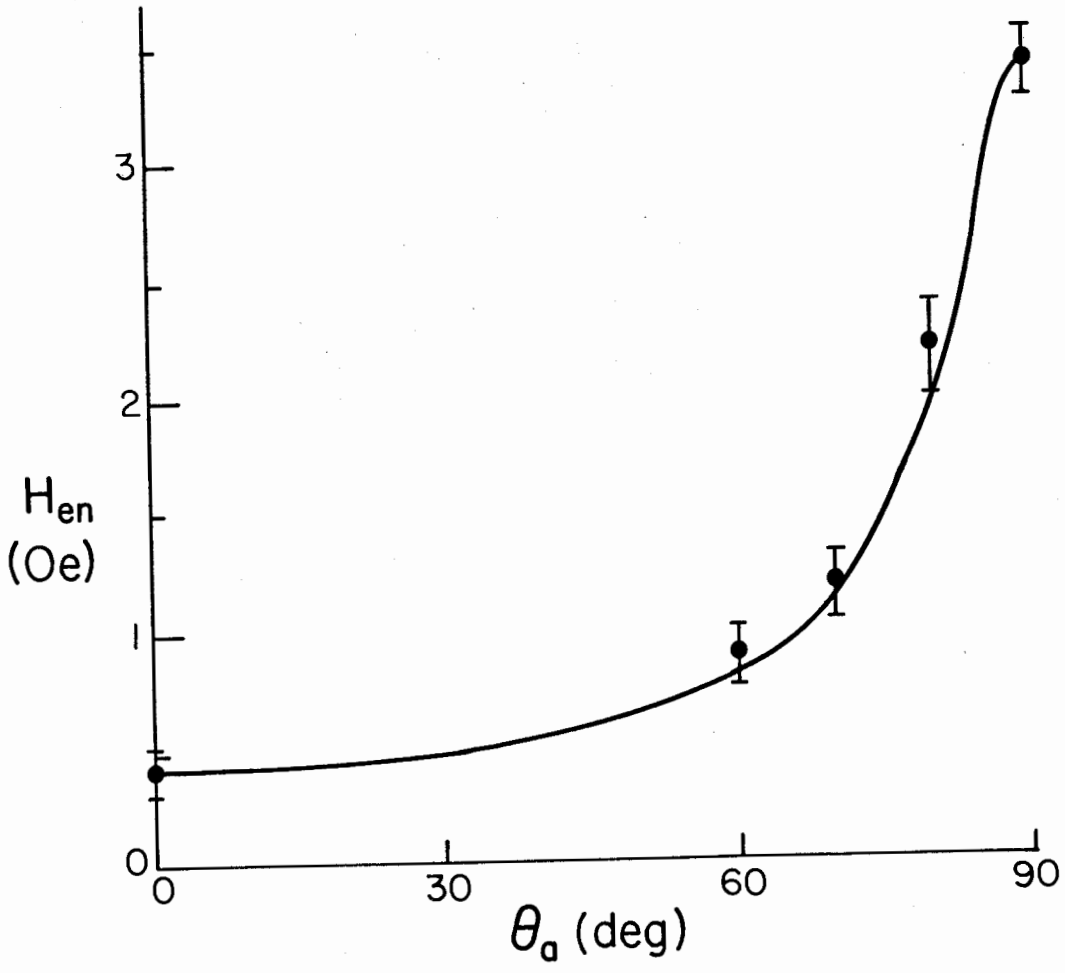

Fig.IV.5- H_{en} vs θ_a for Nb48Ti#2 at $T=(T_c-0.05)K$. Data points and theoretical curve are shown.

Fig.IV.5 shows the data. The theoretical curve is found by solving equation (4-7) for H_a and using 72 Oe/K for H_1. The graph shows H_{en} for a particular temperature ($T=T_c-0.05K$). This is equivalent to plotting $dH_{en}(\theta)/dT$ since

H_{en} vs T is a straight line. Again the measurements agree with the theory. The angular dependence of H_{en} is explained by only considering demagnetization.

Measurements of H_{c1} for Nb-Ti alloys have not been given in the literature. An estimate of κ can be found using measurements of dH_{c2}/dT and normal state resistivity ρ. Using the formula given by Orlando et al,[18] in the dirty limit, κ is given by

$$\kappa = \frac{7.49 \times 10^3}{[4.48 \times 10^4]^{1/2}} \left(\frac{dH_{c2}}{dT}\right)^{1/2}_{T=T_c} \rho^{1/2} \quad . \tag{8}$$

An estimate of dH_{c2}/dT can be obtained using data from Neuringer and Shapira,[19] who give for Nb37%Ti a value $dH_{c2}/dT=-15{,}400$ Oe/K and for Nb56%Ti a value of -25,900 Oe/K. Interpolating between these results gives $dH_{c2}/dT=-20{,}000$ Oe/K for Nb48%Ti. The normal resistivity just above T_c was measured for our annealed Nb48%Ti to be 6×10^{-5} $\Omega\cdot$cm using a four probe technique. Putting these values into the above equation yields $\kappa=39$. Using Ginzburg-Landau theory, the relation between dH_{c1}/dT and dH_{c2}/dT is

$$\frac{dH_{c1}}{dT} = \frac{dH_{c2}}{dT} \frac{1}{2\kappa^2} (\ln \kappa + 0.497) \tag{9}$$

This gives an estimated value for dH_{c1}/dT of 27 Oe/K.

The measured value of $dH_{eni}/dT=72$ Oe/K is much larger than the expected dH_{c1}/dT value. Evidently there is some mechanism which delays the entry of flux into the superconductor. If the cause of the delayed flux

was a surface effect, it should have a different magnitude for different sizes and shapes of surfaces. The four measured values of dH_{eni}/dT are the same. This would indicate that the cause of the delayed flux entry was a bulk effect rather than a surface effect. In addition, the appearance of the surfaces was dull and the surface barrier to flux entry is maximum for shiny surfaces, so the effect of a surface barrier is expected to be small. As pointed out in Chapter II, the presence of delayed flux entry is accompanied by an irreversible magnetization curve. Curves for the Nb48%Ti were found to be very irreversible (see Fig.IV.3), whereas, for an ideal superconductor, all the flux should be expelled below $T(H_{c1})$. The measrurement of H_{en}, in this case is not just a measurement of H_{c1} but it also includes the effects of flux pinning, which appear to be isotropic.

V. Results - Anisotropic Superconductor

Samples

Single crystals of 2H-$NbSe_2$ were obtained from Dr. R. F. Frindt (batch R). The crystals were grown by the iodine vapor transport method.[20] The structure of $NbSe_2$ is of electrically conducting layers which are loosely bound together by van der Waals gaps. The spacing of the layers is about 6 A. The crystals grow in the shape of thin platelets with the layers parallel to the broad surfaces of the platelet. Samples were carefully chosen single crystals with smooth surfaces and uniform thickness. $NbSe_2$ is a soft substance and the crystals were handled with due care. Each sample was weighed on a Cahn model G-2 electrobalance. The dimensions of the broad surfaces were measured under a microscope. Using the measured area and mass of a crystal, its thickness was calculated, taking the density of $NbSe_2$ to be 6.45 g/cc. The following convention was used when labeling the dimensions of the broad surfaces. As shown in Fig.V.1a, for a magnetic field applied parallel to the layers, the height h of the crystal is the dimension in the direction of the applied field, whereas the width w of the crystal is taken to be the dimension of the broad surface perpendicular to the applied field. Fig.V.1b shows how h and w change for a different orientation of the applied field (still parallel to the layers). Extensive magnetization measurements were made on three crystals which will be called $NbSe_2$#1, $NbSe_2$#2, and $NbSe_2$#3. Fig.V.2 and Table V.1 show the shapes and the dimensions of the samples.

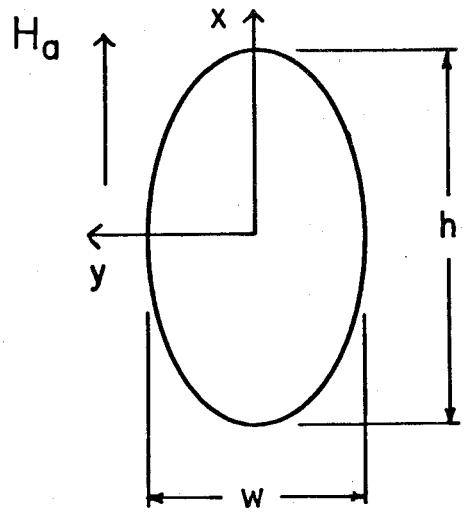

Fig.V.1a- Sketch of a sample in a field applied parallel to the layers. h is the dimension of the sample parallel to the field.

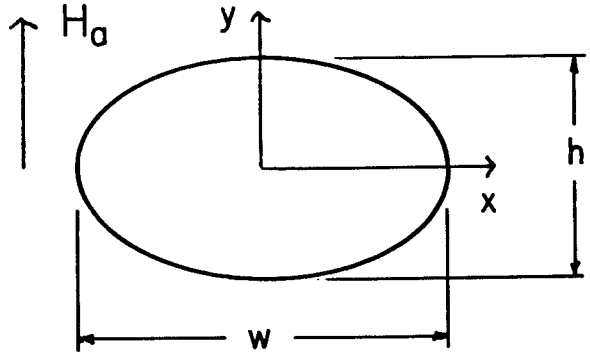

Fig.V.1b- Sketch showing how h changes when the sample is rotated from its position in Fig.V.1a. The applied field is still parallel to the layers.

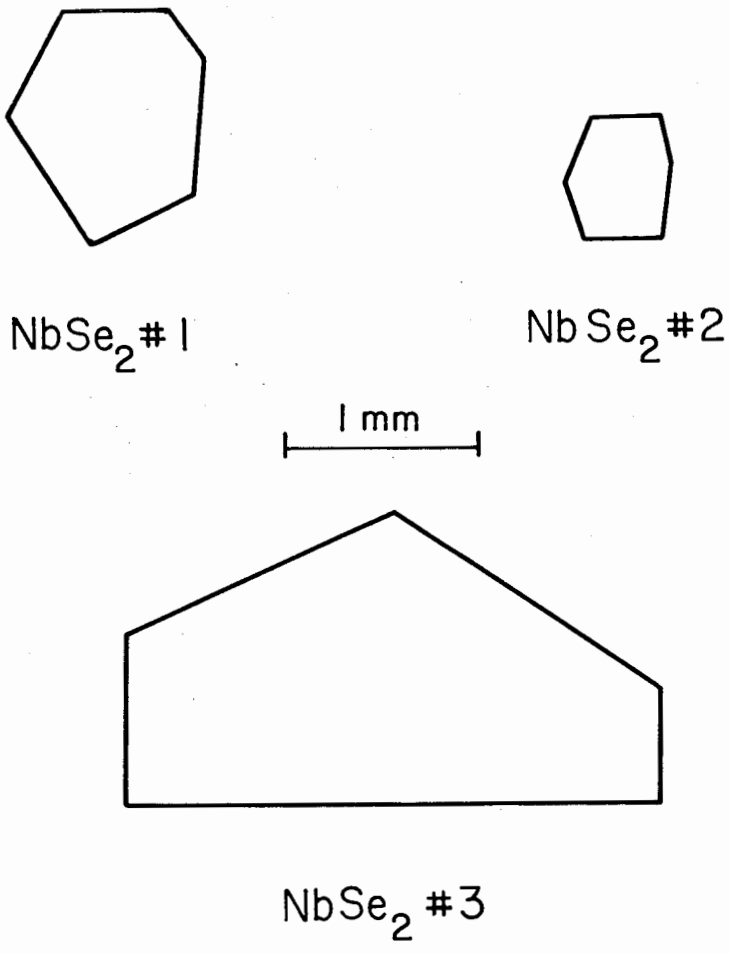

Fig.V.2- Sketches of the shapes of the three $NbSe_2$ samples drawn approximately to scale.

Demagnetization

Demagnetization factors for the $NbSe_2$ samples were found from the measured transition heights using the method described in Chap.IV. The results are summarized in Table V.1. Fig.V.3 shows measured transition heights for $NbSe_2$#1 plotted against the angle of the applied field. (When θ_a=0 the applied field is perpendicular to the crystal layers.) The solid curve shows the calculated transition heights. There is good agreement between the measurements and the calculation, but the measured points lie slightly below the calculated curve. This, again, is probably due to the dipole assumption used in the calculation.

Unlike the Nb48%Ti samples, which were shaped into ellipsiods, the $NbSe_2$ samples are somewhat irregular in shape. When a magnetic field is applied perpendicular to the platelets the demagnetizing factor will be somewhat smaller at corners than it is in the bulk.[3] The average demagnetizing effect, which is measured by the transition heights, will be somewhat smaller than the calculated demagnetizing effect using the average sample dimensions. The samples $NbSe_2$#1 and #2 were not far from ellipsoidal in shape and the measured demagnetizing effect in the z-direction was about 10% smaller than the calculations. The shape of $NbSe_2$#3 deviates considerably from an ellipsoid. The internal field near the edges will be smaller than the field near the center of the platelet. Since the flux lines enter at the edges, a calculation of internal H_{en} due to demagnetizing effects will overestimate it for $NbSe_2$#3.

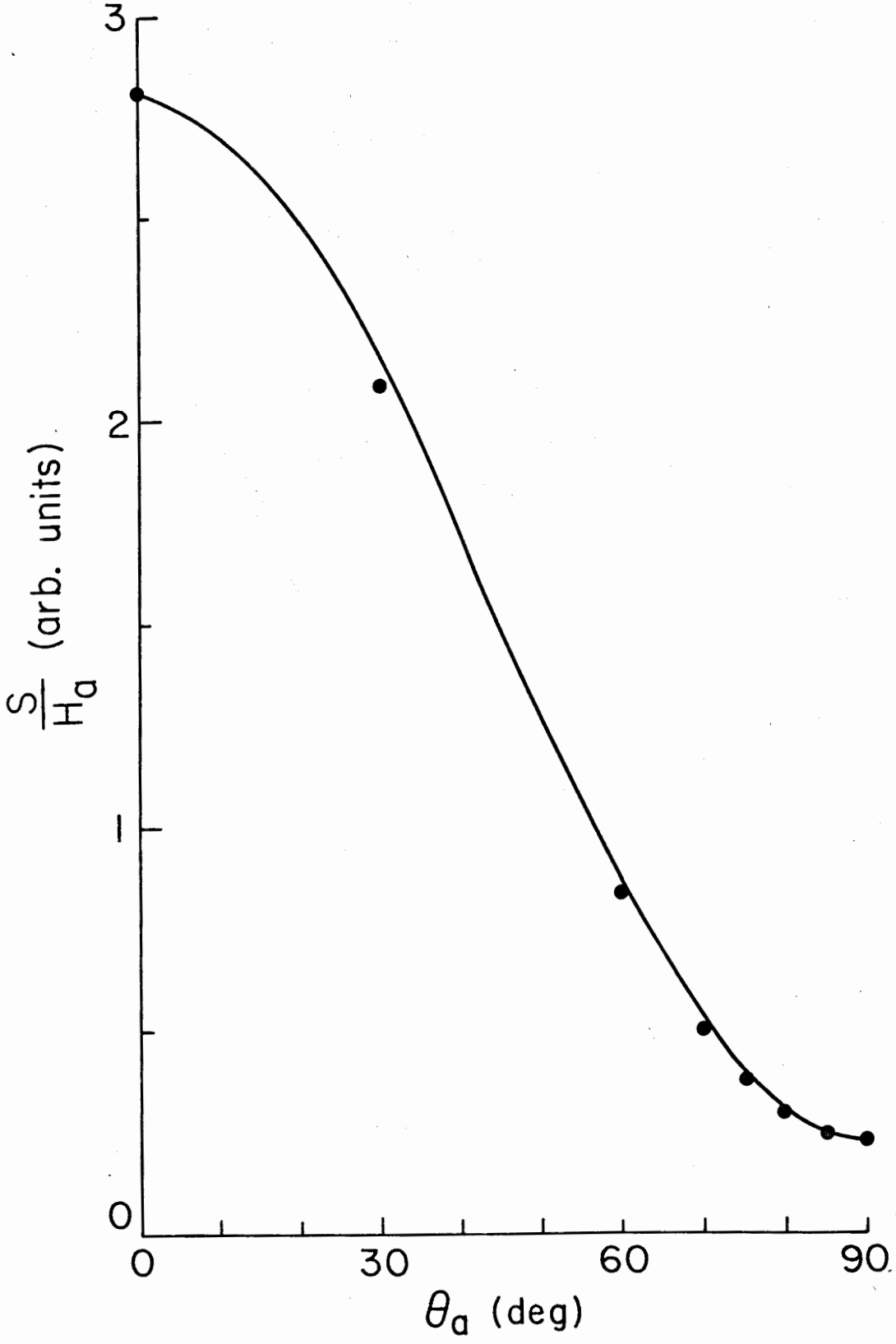

Fig.V.3- Measured and calculated transition heights for $NbSe_2$#1.

Entrance Field Measurements

Temperature induced magnetic transitions were recorded for the $NbSe_2$ samples in the same way as for the Nb48%Ti samples. A sample would be cooled in zero field, then a constant field applied and the temperature of the sample raised slowly. Fig.V.4 shows examples of magnetic transitions for $NbSe_2$#3 with the applied field parallel to the layers. As for the Nb48%Ti, these transitions were found to be irreversible. Upon cooling the sample in a constant field most of the original flux through the sample remained trapped. The amount of flux trapped depended on the direction of the applied field relative to the crystal layers. (This is not shown in the figure.) $T(H_{en})$ is the point where a curve breaks away from a lower field curve. For each fixed angle of the sample in the applied field, entry points $T(H_{en})$ were found for a number of applied fields. The plot of H_{en} vs T, Fig.V.5, shows the expected linear relationship, near T_c. Values of dH_{en}/dT for the applied field perpendicular to and parallel to the layers for the three samples are given in Table V.2. A graph showing the angular dependance of H_{en} for $NbSe_2$#3 is shown in Fig.V.6. In order to obtain the angular dependence, the sample was rotated in steps from being perpendicular with respect to the field to being parallel. In Fig.V.6, for the sample parallel to the field, h was the largest sample dimension as shown in Fig.V.1a. Data for the same crystal are given in Fig.V.7, but here the sample rotation is done so that when it is parallel to the field, h is the smaller dimension as in Fig.V.1b. Data for $NbSe_2$#1 and #2 are shown in Fig.V.8 and Fig.V.9. In both cases h is the larger dimension.

Table V.1

The approximate largest and smallest distance across the $NbSe_2$ samples are given for the two definitions of h and w. Also given are the sample thickness t and area of the broad surfaces A. The last columns give the measured demagnetization factors.

sample	w(mm)	h(mm)	t(mm)	A(mm^2)	1/1-L	1/1-M	1/1-N
#1	0.77	1.15	0.041	0.877	1.04	-	12.82
#2	0.63	0.43	0.014	0.27	1.02	1.03	19.2
#2	0.43	0.63					
#3	2.7	1.2	0.028	3.1	1.01	1.02	29
#3	1.2	2.7					

Table V.2

The measured $H_{en}(0)$ and $H_{en}(90)$ for the $NbSe_2$ samples along with the calculated internal fields, $H_{eni}(0)$ and $H_{eni}(90)$. The rows correspond to the rows in Table V.1.

sample	$dH_{en}(0)/dT$	$dH_{en}(90)/dT$	$dH_{eni}(0)/dT$	$dH_{eni}(90)/dT$
#1	11.5(Oe/K)	47.0(Oe/K)	150(Oe/K)	48.9(Oe/K)
#2	8.075	50.7	155	52.2
#2	-	48.45	-	49.4
#3	6.035	46.75	175	47.7
#3	-	42.5	-	42.9

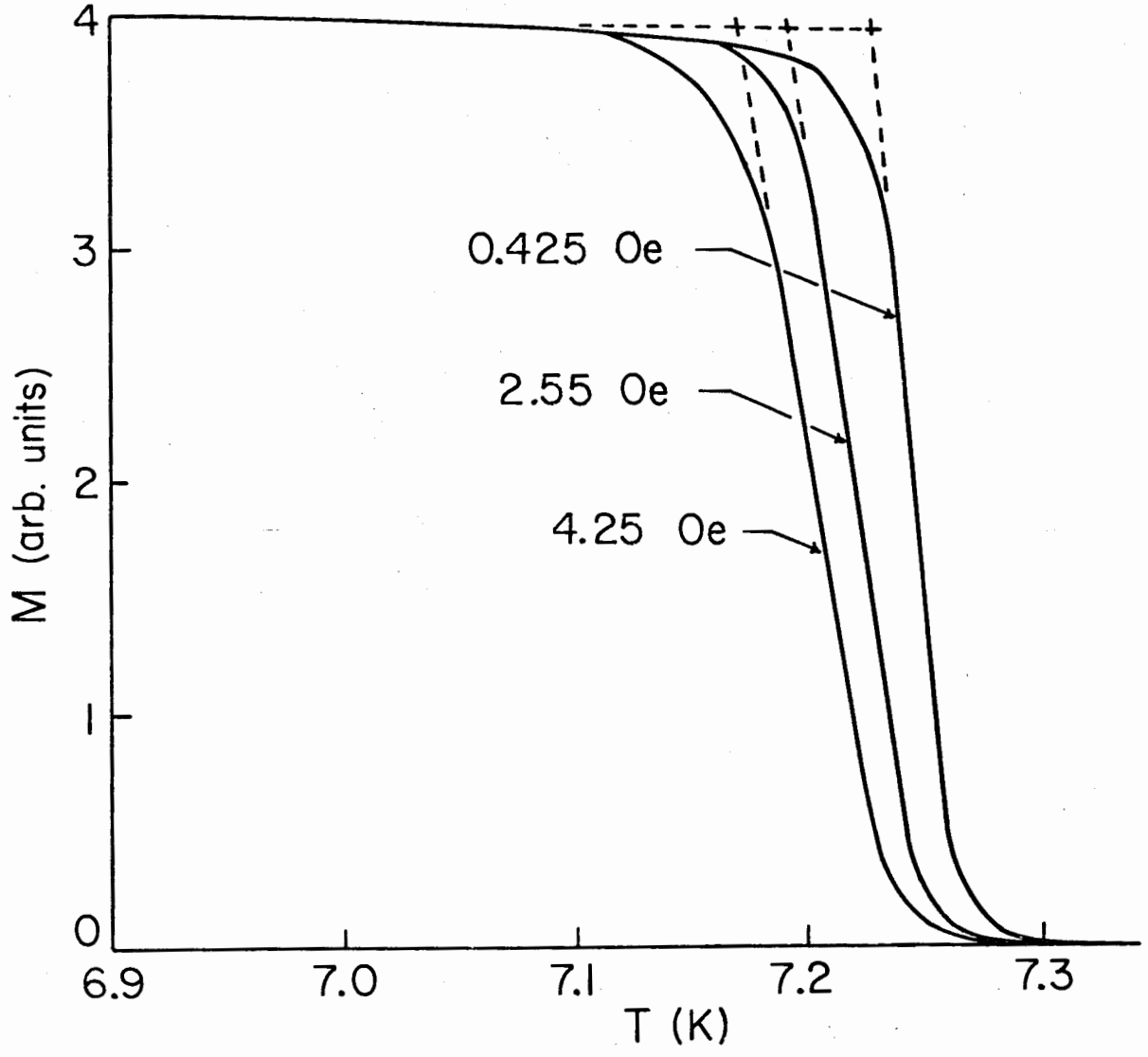

Fig.V.4- Magnetic transitions for $NbSe_2$#3 for θ_a=90.

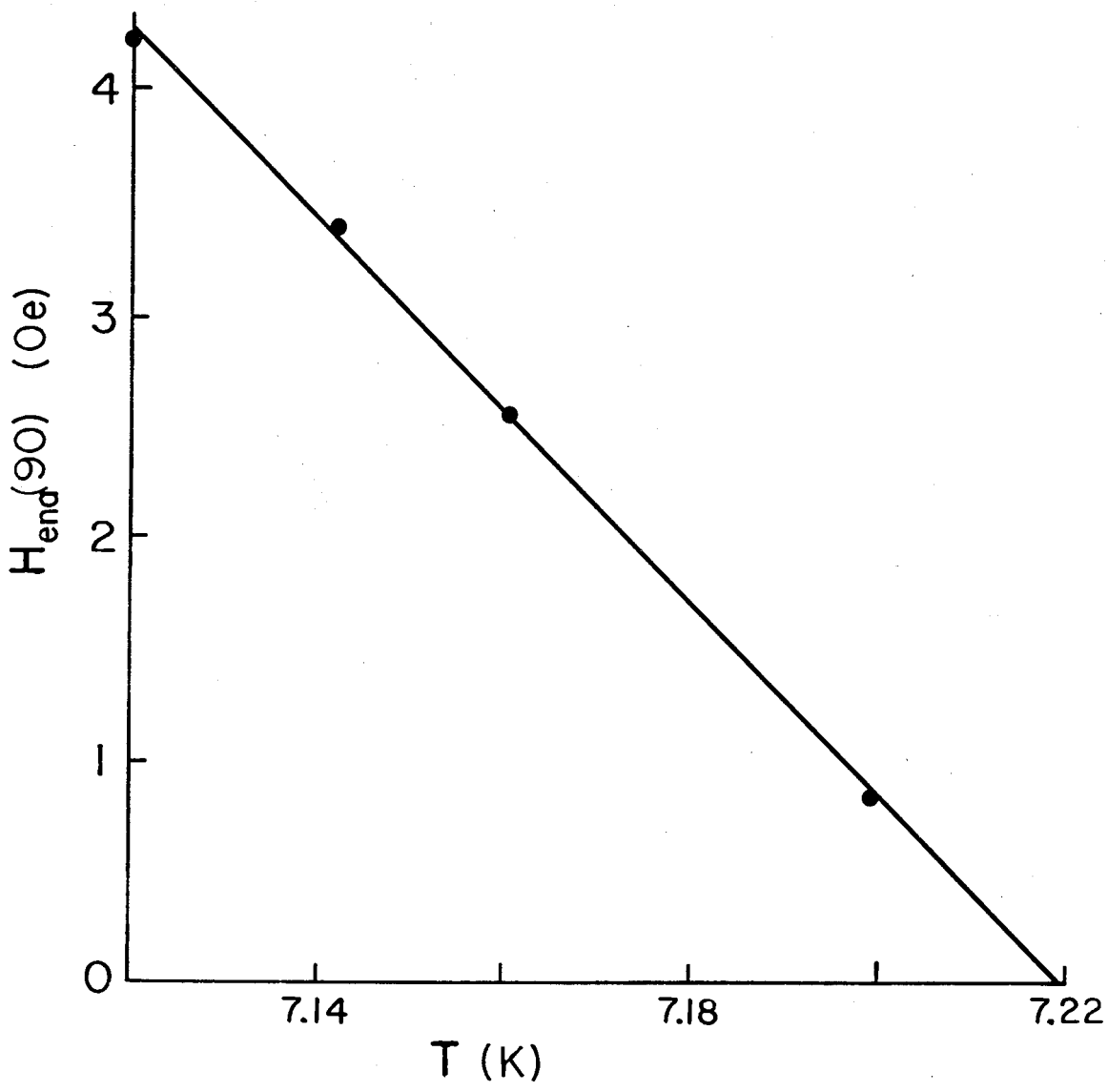

Fig.V.5- Measured H_{en} vs T for $NbSe_2$ #3 for θ_a=90, with a straight line drawn through the data.

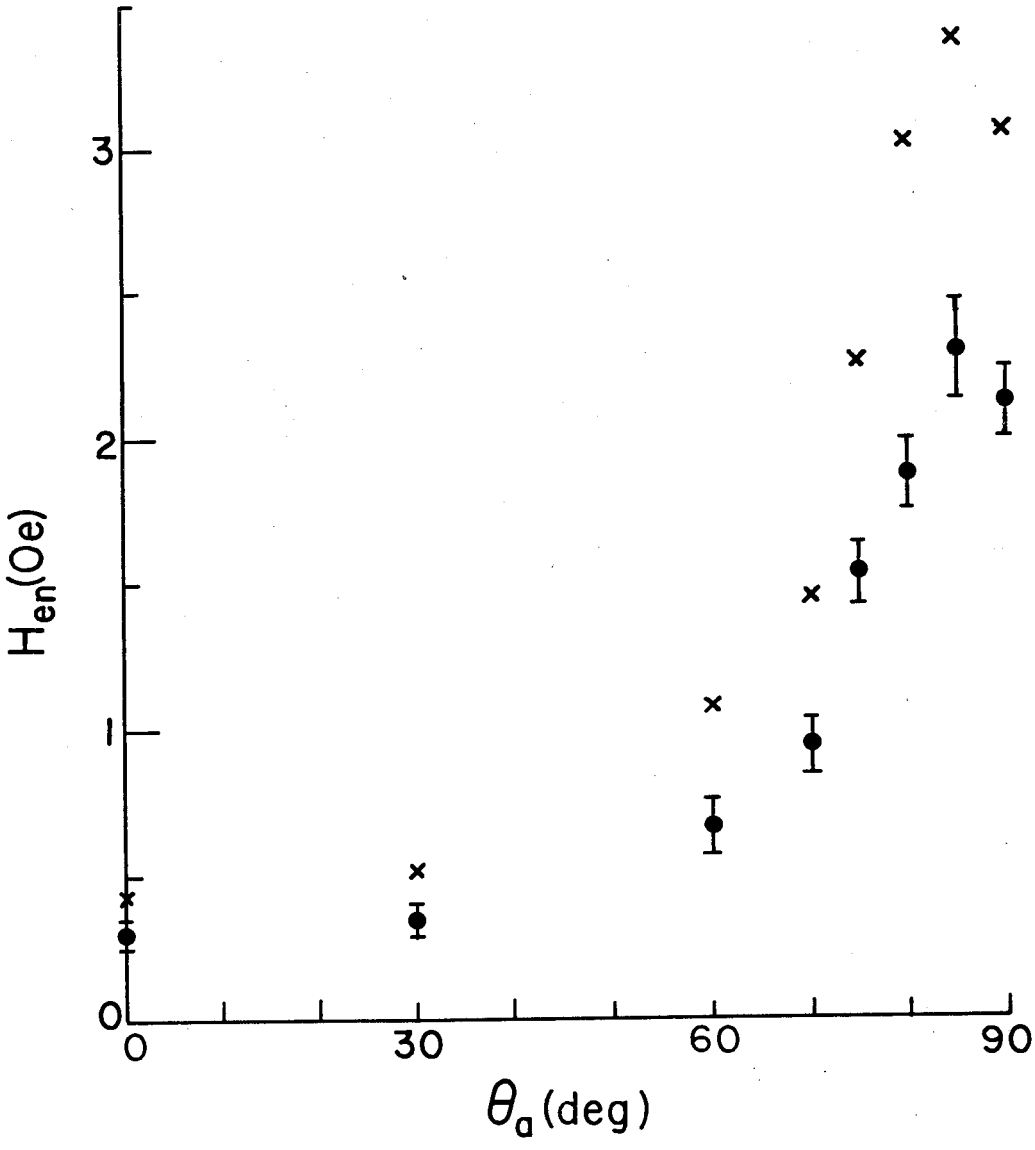

Fig.V.6- Experimental H_{en} (dots) and H^*_{en} (crosses) for $NbSe_2$ #3 with h equal to the largest sample dimension.

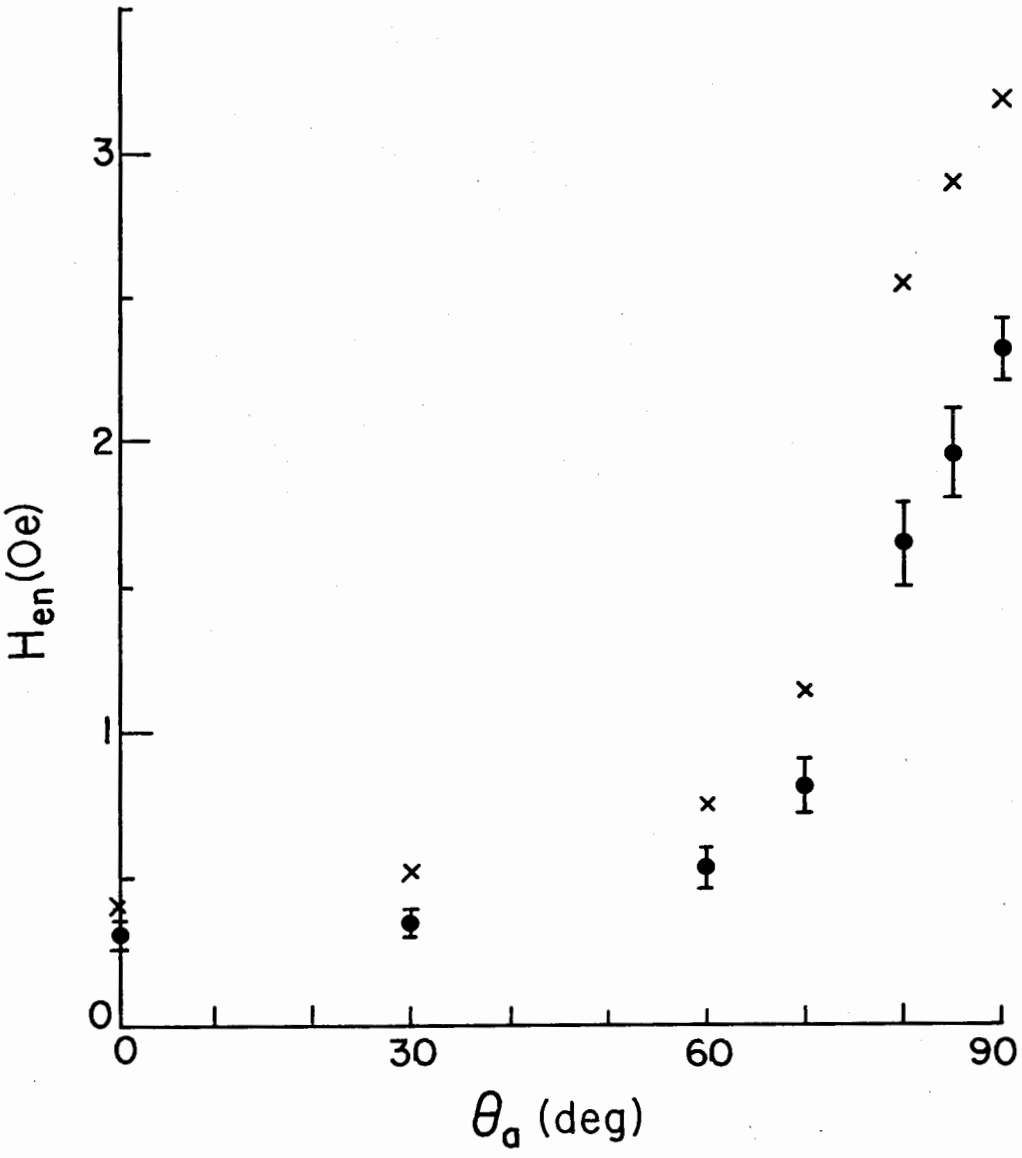

Fig.V.7- Experimental H_{en} (dots) and H^*_{en} (crosses) for $NbSe_2$#3 with h being the smaller sample dimension.

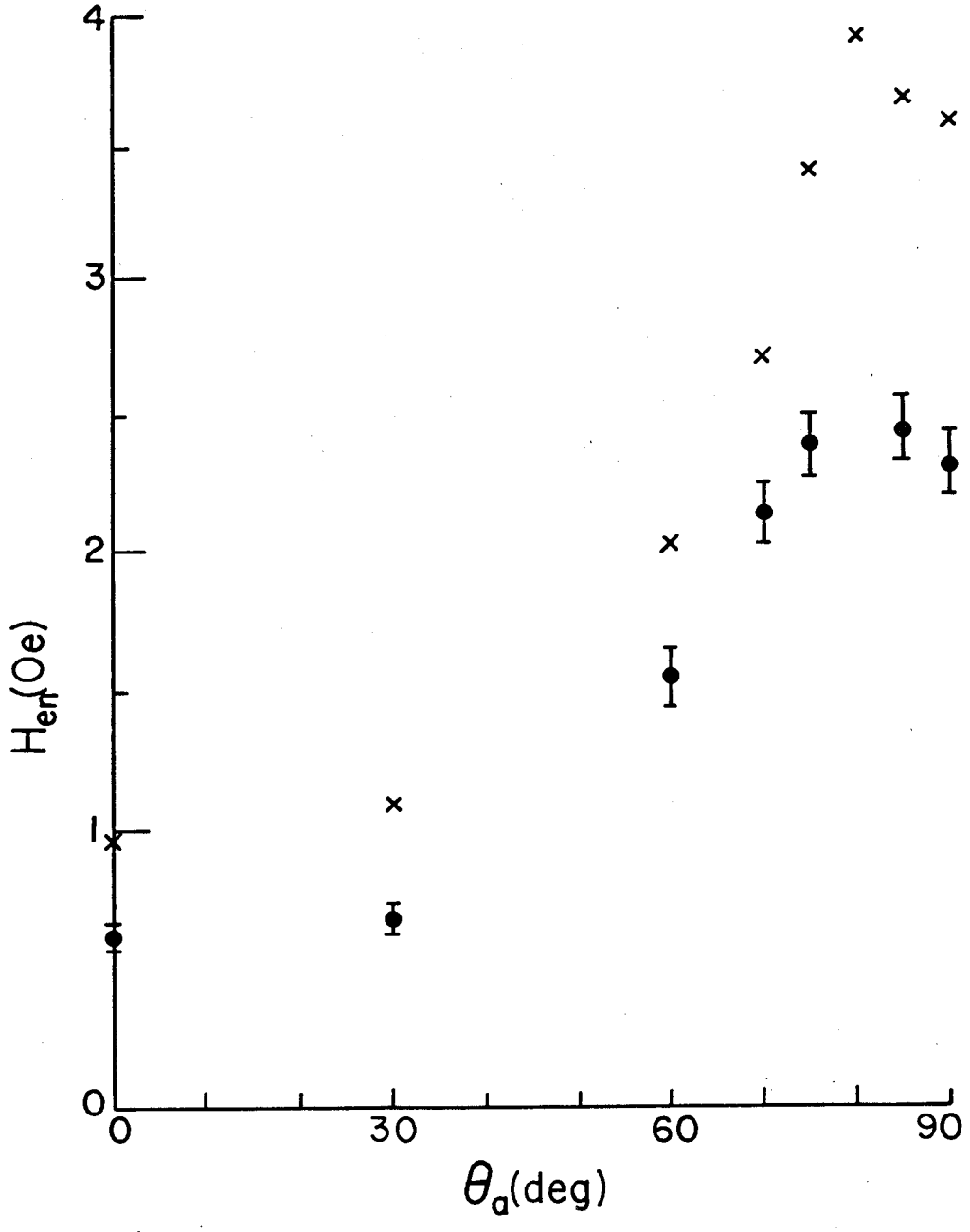

Fig.V.8- Experimental H_{en} (dots) and H^*_{en} (crosses) for $NbSe_2$#1. H_{en} was found by both field sweep and temperature sweep techniques.

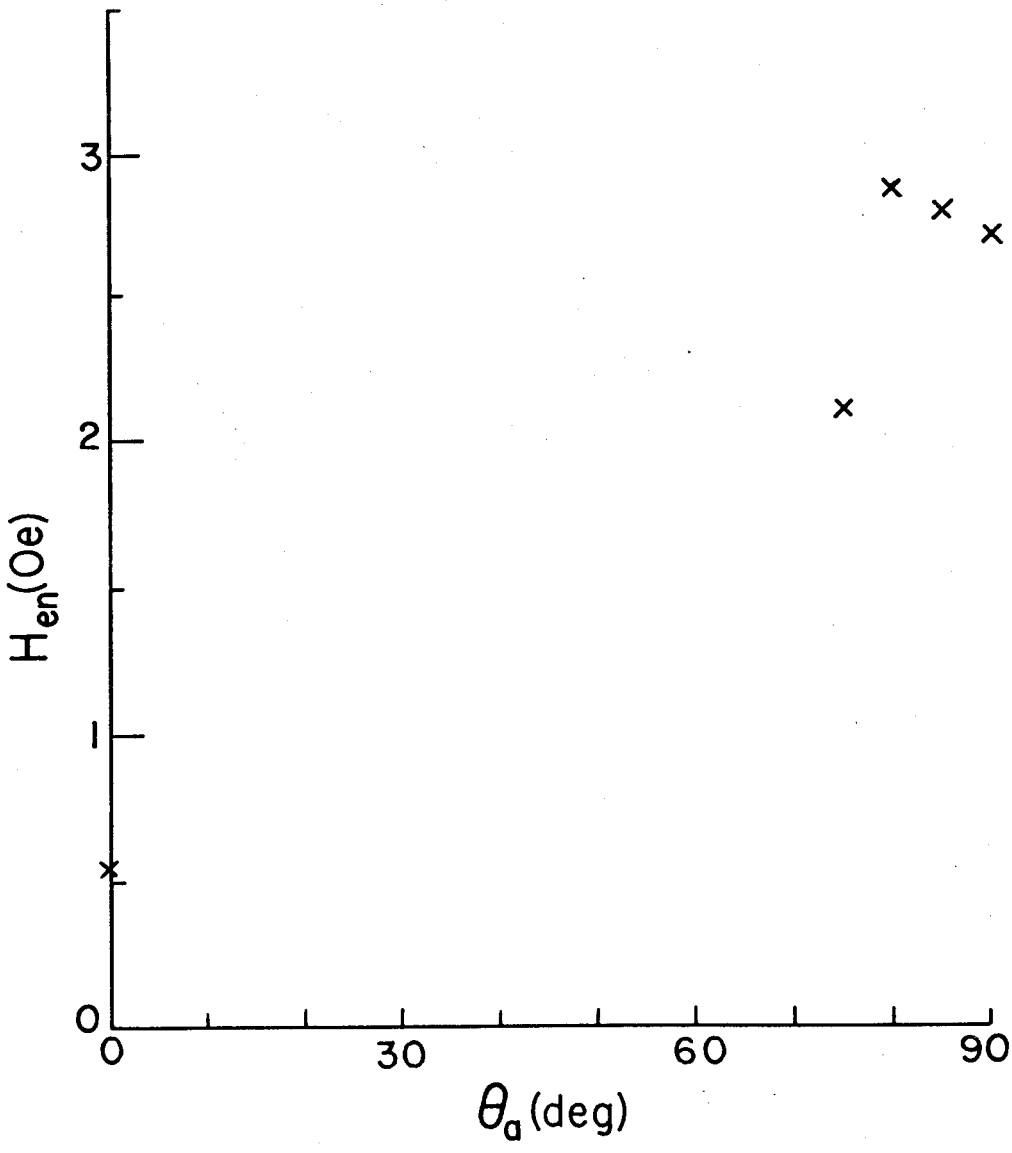

Fig.V.9- Experimental H^*_{en} for $NbSe_2$#2.

There still may be some concern that the measured values of H_{en} are lowered by inhomogenious regions of the sample or by irregularities in the shape of the sample. An indication of how the flux enters the bulk of a sample is found by considering the main region of the transition where a large quantity of flux is entering the sample. This part of the transition is linear and can be extrapolated back to lower temperatures as shown by the dotted lines in Fig.V.4. The point where this extrapolation crosses an extrapolation of the low temperature curve gives a value which will be called $T(H^*_{en})$. The quantity H^*_{en} will be somewhat larger than the actual critical entry field H_{en}. H^*_{en} should be related to the bulk properties of the crystal. (Size and shape are included in "bulk properties".) The slopes dH^*_{en}/dT can be found near T_c. These results are shown for $NbSe_2$#3 in Fig.V.6 and Fig.V.7, plotted against the angle of the applied field. The data for H^*_{en} show the same features as those for H_{en} but are larger by about a factor of 1.4. This would indicate that the features of the measured H_{en} are not due to inhomogeneities of composition or irregularities in shape of the sample. The curve $H_{en}(\theta_a)$ is a property of the whole crystal (ie. a bulk property).

A field sweep method was also used to measure H_{en}. The sample was cooled in zero field to a temperature below T_c. The sample is then held at a fixed temperature while a gradually increasing field is applied. The magnetization is measured as a function of the applied field. The ac magnet was used to apply the field as described in Chapter III. There was considerably more noise in the SQUID signal in the field sweep method than in the constant field method. Examples of magnetization curves for $NbSe_2$#1 at a fixed angle are shown in Fig.V.10. Ideally, for low fields, when the

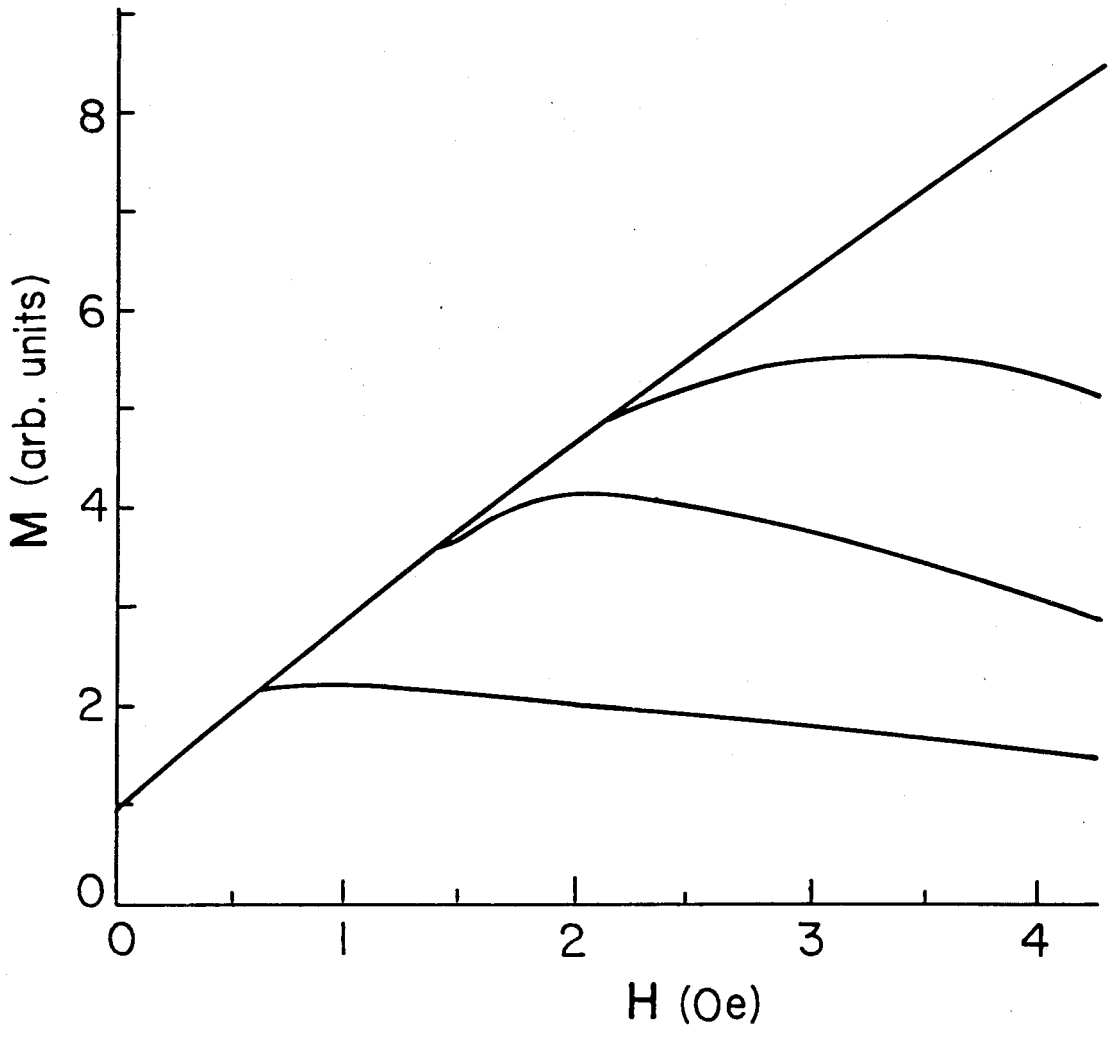

Fig.V.10- Measured magnetization curves for $NbSe_2$#1 with the applied field perpendicular to the layers.

sample is in the Meissner state, the magnetization vs field would give a linear plot. The non-linearity of the low temperature curve is due to a background signal from the magnetometer itself and was present even in the absence of a sample.

To find H_{en} from the field sweep data, the curve for the lowest temperature, at which the sample was in the Meissner state, was used as a base. The value of H_{en} is taken from where a fixed temperature curve breaks away from the Meissner state curve. The values of H_{en} found using the field sweep method agreed within errors with the values of H_{en} found using the temperature sweep method. The results for $H_{en}(\theta_a)$ for $NbSe_2$#1 are shown in Fig.V.8. Also in Fig.V.8 are the results of $H^*_{en}(\theta_a)$ found by extrapolation of the bulk of the temperature swept transitions. H_{en} is again smaller than H^*_{en} by a constant factor.

The temperature induced transition curves, Fig.V.4, show a slowly decreasing magnetization even before $T(H_{en})$ is reached. This is probably due to the temperature dependence of the penetration depth. The penetration depth will reduce the volume in which flux is excluded in the Meissner state. When the applied field is parallel to the platelet, the thickness of the Meissner region will be reduced by an amount $2\lambda(T)$. Where λ is the distance the induction penetrates into the broad surfaces of the platelets in a direction perpendicular to the crystal layers. The surface area of the edges of the platelets are small and the penetration here is neglected. For fields smaller than H_{en}, the magnetization should be proportional to $(t - 2\lambda(T))$, where t is the platelet thickness. Near T_c the penetration depth has the form[21]

$$\lambda(T) = \frac{1}{\sqrt{2}} \lambda(0) \left(\frac{T_c}{T_c - T}\right)^{1/2} , \qquad (1)$$

where $\lambda(0)$ is the London penetration depth at T=0. The magnetization curve for $NbSe_2$#1 did fit this functional relationship giving $\lambda(0)$=110 nm. Finley and Deaver Jr. measured λ for $NbSe_2$ using a SQUID magnetometer.[22] Their result for the penetration depth perpendicular to the layers was 124 nm. Using specific heat measurements, Schwall et al[8] calculated λ to be 115 nm. This agreement confirms that the decrease of magnetization below H_{en} is due to the increasing penetration depth.

Comparison of Results and Theory

Table V.2 gives a summary of the data for the three $NbSe_2$ samples. The internal entry field parallel to the layers $H_{en}(90)$ varies, not only from crystal to crystal, but for the same crystal with the field in the x or the y direction (see Fig.V.1). This implies that the cause of the different values for $H_{en}(90)$ would not be differences in composition. Keeping the thickness of a crystal constant, $H_{en}(90)$ gets larger as the ratio h/w gets smaller. This is seen by looking at two values of $H_{en}(90)$ for $NbSe_2$#2 or #3. Comparing all of the values of $H_{en}(90)$ for the three crystals, it would appear that $H_{en}(90)$ gets larger as t gets smaller. By trial and error it was found that a systematic result is achieved by plotting $H_{en}(90)$ vs (h/w)(A/t), which is shown in Fig.V.11. Considering the size of the error bars, the data points fall on a remarkably smooth curve. This would suggest that the errors are over-estimated. However, the exact point of $T(H_{en}(90))$ on the magnetization curves is difficult to choose and the author feels the quoted errors are realistic. The general trend which the data implies is for $H_{en}(90)$ to increase as the size of a crystal decreases, while $H_{en}(90)$ decreases slowly or perhaps approaches a constant

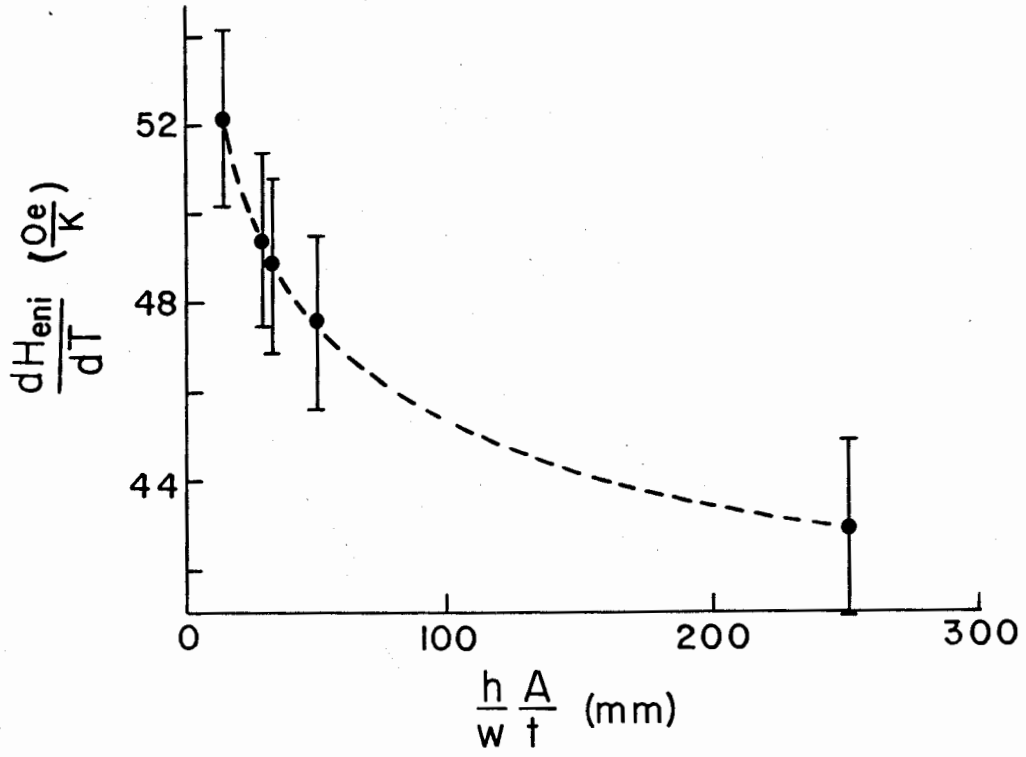

Fig.V.11- Graph showing the dependence of $dH_{eni}(90)/dT$ on the size of $NbSe_2$ crystals. A smooth curve is drawn to connect data points. H_{eni} is the internal field corresponding to H_{en}.

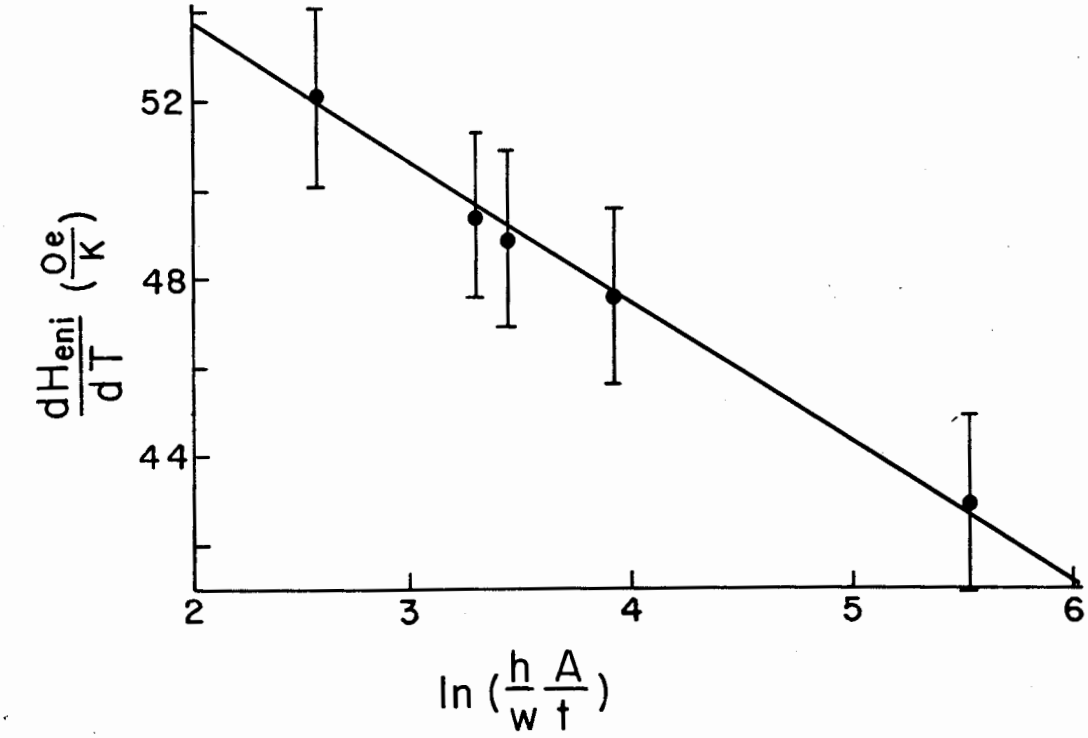

Fig.V.12- Graph showing the approximate empirical relation between dH_{eni}/dT and crystal size for $NbSe_2$, for the data from Fig.V.11.

as the size of a crystal increases. The shape of the curve of $H_{en}(90)$ vs $(h/w)(A/t)$ suggests a logarithmic dependence. A plot of $H_{en}(90)$ vs $\ln(h/w)(A/t)$ is given in Fig.V.12. The functional dependence is approximately logarithmic, although somewhat uncertain because of the large error bars and the small range of crystal sizes. There is, at present, no theoretical explanation for this relationship.

The calculated internal entry fields perpendicular to the crystal layers $H_{en}(0)$ also show some variation. The demagnetizing effect for a perpendicular field has large uncertainties, especially for $NbSe_2$ #3, and this can account for the different values completely. The results for $NbSe_2$ #1 and #2 of approximately 150 Oe/K will be taken as the best value of $H_{eni}(0)$.

Predictions for the value of H_{c1} can be made using measurements of H_{c2} and κ found in the literature. Using Ginzburg-Landau theory as in Chapter IV,

$$\frac{dH_{c1}}{dT} = \frac{\frac{dH_{c2}}{dT}(\ln\kappa + 0.497)}{2\kappa^2} \quad . \qquad (2)$$

Schwall, Stewart, and Geballe[8] use specific heat measurements to find $dH_{c2}(90)/dT$=25,700 Oe/K, $dH_{c2}(0)/dT$=6450 Oe/K, $\kappa_{//}$=54, and $\kappa_{\perp}$=13.5. Putting these values into the equation for dH_{c1}/dT gives $dH_{c1}(90)/dT$=20 Oe/K and $dH_{c1}(0)/dT$=55 Oe/K. As for the Nb48%Ti, measured values of the internal fields for $NbSe_2$, $dH_{en}(90)/dT$=50 Oe/K and $dH_{en}(0)/dT$=150 Oe/K, are larger than the expected values. The cause of this delayed flux entry would again be the presence of flux pinning forces.

There is a theoretical model (Chapter II) which describes quite

successfully, the delayed flux entry caused by flux pinning. It is called the critical state model.[3,10,11] The critical state model has been used to calculate the critical current density (which is directly related to flux pinning) for large applied fields using a constant temperature field sweep technique. In the critical state model, irreversible transport currents provide shielding from the applied field in addition to the shielding provided by the reversible Meissner currents. Unfortunately, a temperature dependent theory has not been developed. A quantitative analysis of the data reported here cannot be done at present.

A description of how the flux enters would be helpful in understanding anisotropic superconductors. Although the effects of reversible magnetization and flux pinning can not be separated here, measurement of H_{en} does give the point when flux enters a sample. It is useful to compare the theoretical dependence of H_{c1} on the angle of the applied field θ_a and the measured angular dependence of H_{en}. Graphs comparing the H_{c1} theory, outlined in Chapter II, and the H_{en} data are given in Figs.V.13, 14, 15, and 16, using Schwall's values of $\kappa_\perp=13.5$ and $\sqrt{\epsilon}=0.25$. The figures show that the actual entry field differs in behavior from the theoretical H_{c1}. By using a smaller value for ϵ, i.e. higher anisotropy, Klemm and Clem's theory does show a break in the curve, Fig.V.14. But the shape of the smaller ϵ curve does not agree with the shape of the measured curve, so it is reasonable to take Schwall's measured value for ϵ as being correct for $NbSe_2$. Since the measured H_{en} has a larger anisotropy than the calculated H_{c1}, the flux pinning which is present in the real crystals, must add to the anisotropy.

A simple model can be developed to show how the fluxoids might enter

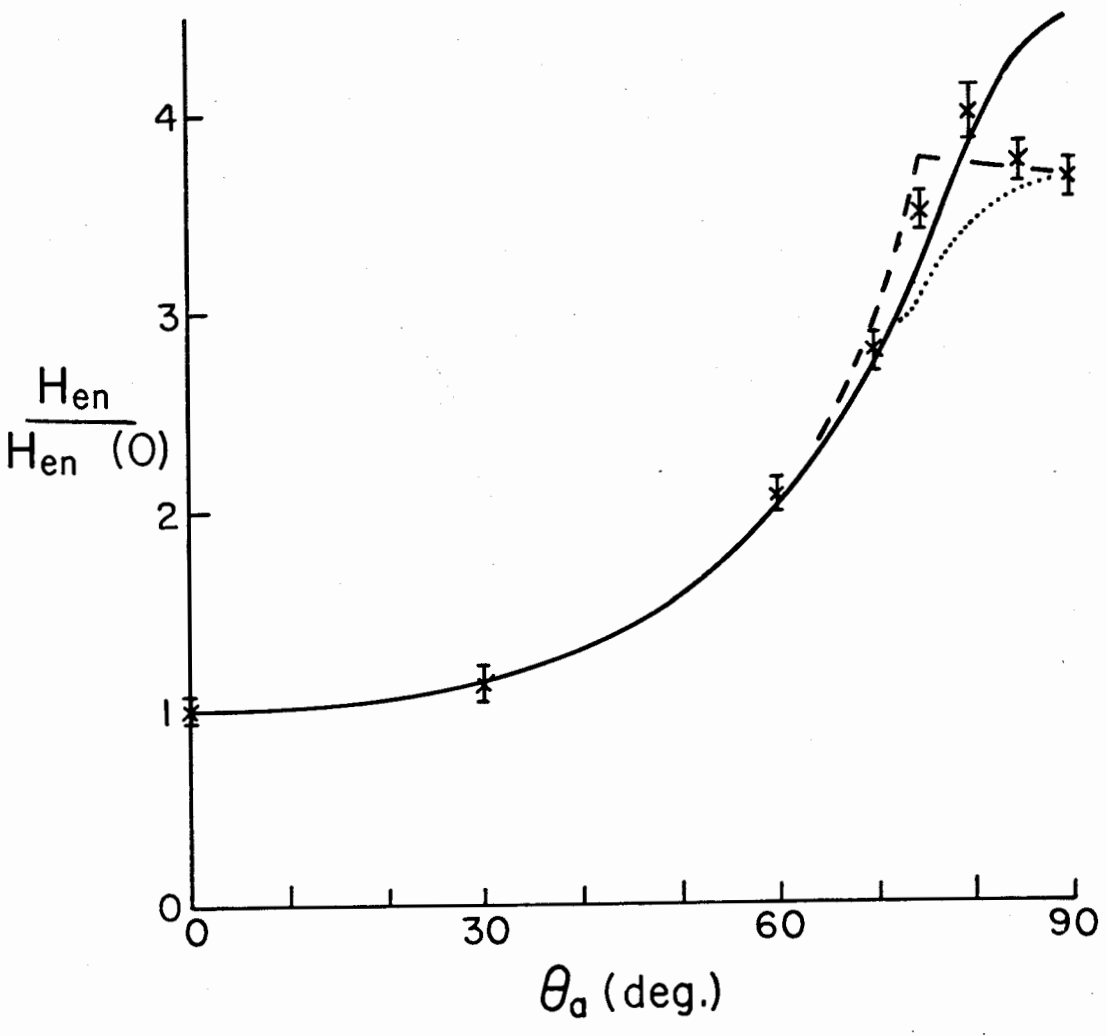

Fig.V.13- Experimental H_{en} data points for $NbSe_2$ #1 compared with Klemm and Clem's theory[1] for $\kappa_\perp = 13.5$ and $\sqrt{\epsilon}=0.25$ (solid) and $\sqrt{\epsilon}=0.19$ (dotted), and with the parallel/perpendicular model (dashed).

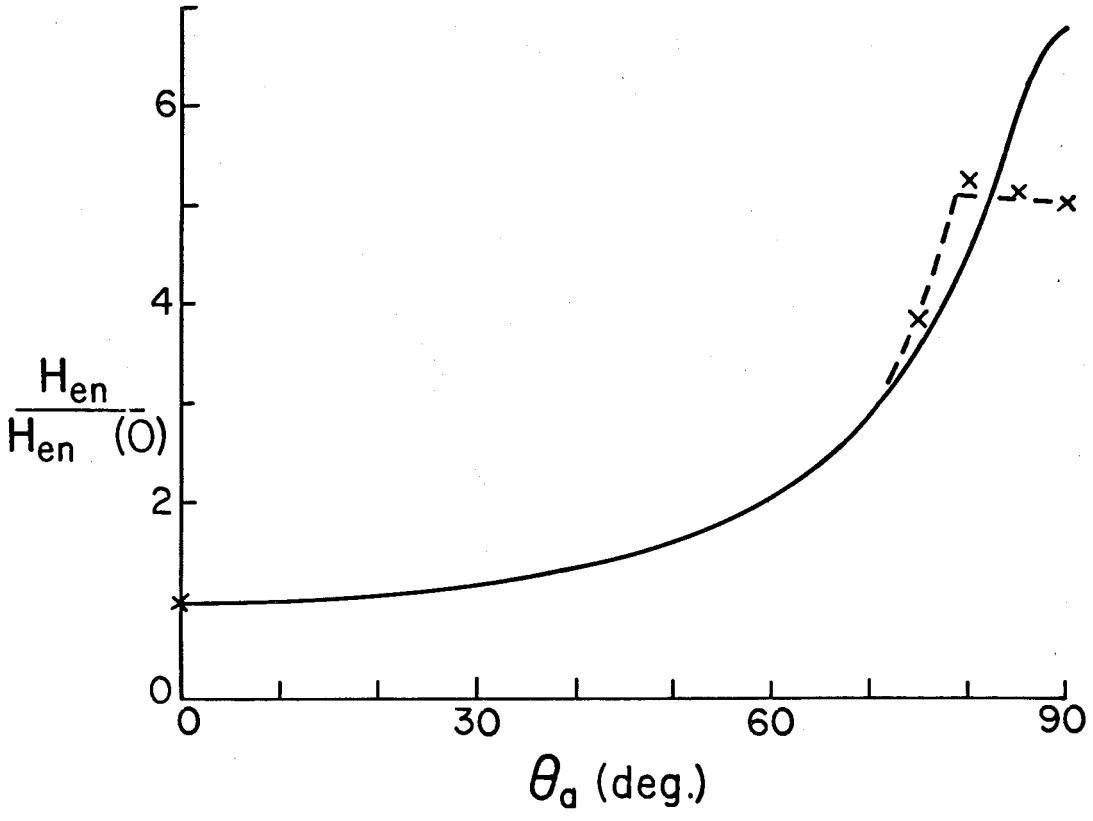

Fig.V.14- Experimental H^*_{len} data for $NbSe_2$ #2 compared with Klemm and Clem's theory for $\kappa_\perp = 13.5$ and $\sqrt{\varepsilon} = 0.25$ (solid), and with the parallel/perpendicular model (dashed).

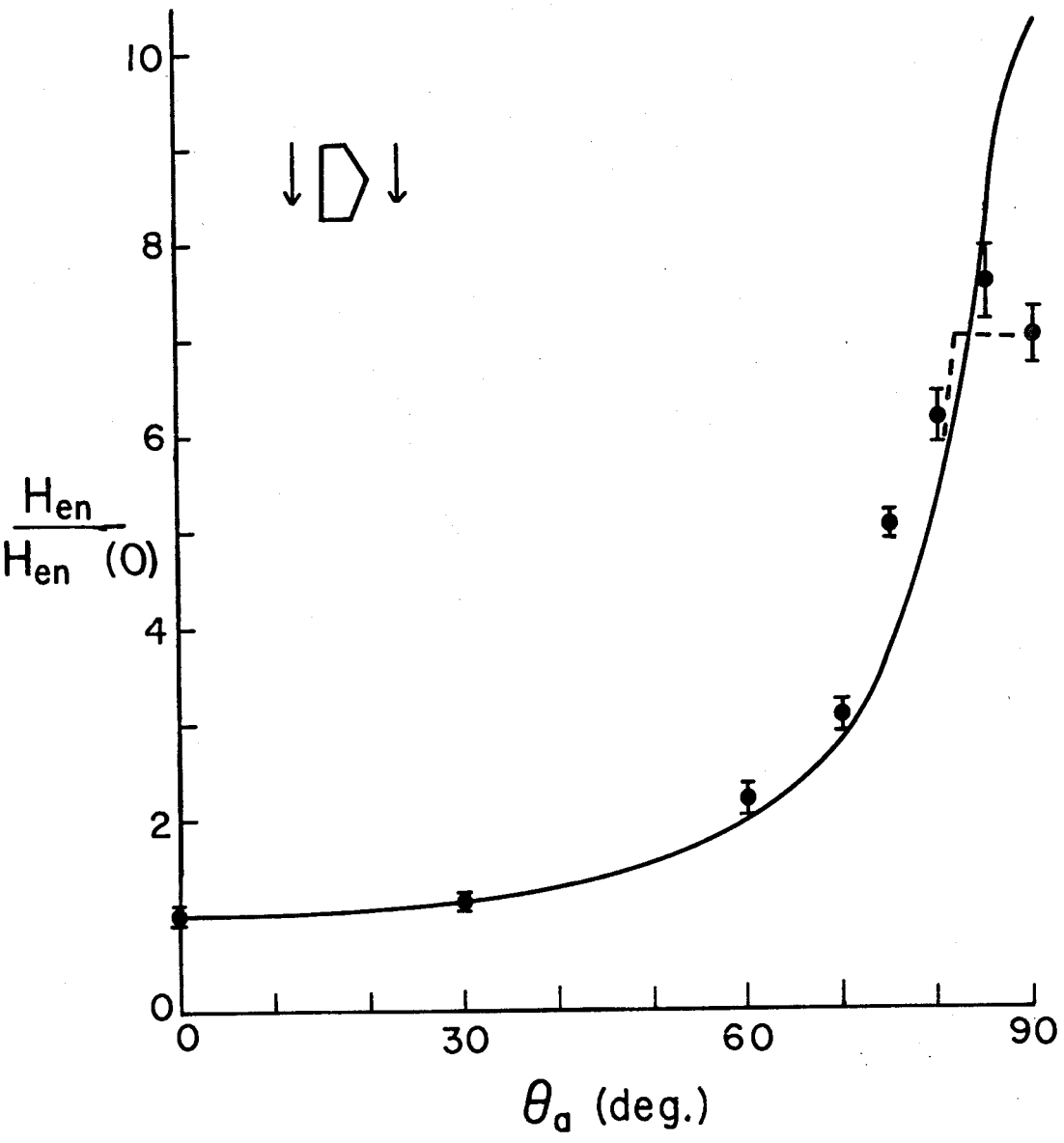

Fig.V.15- Experimental H_{en} data points for $NbSe_2$#3, with h equal to the long sample dimension, compared with Klemm and Clem's theory[1] for $\kappa_\perp$=13.5 and $\sqrt{\epsilon}$=0.25 (solid), and with the parallel/perpendicular model (dashed). The insert shows the applied field direction for θ_a=90.

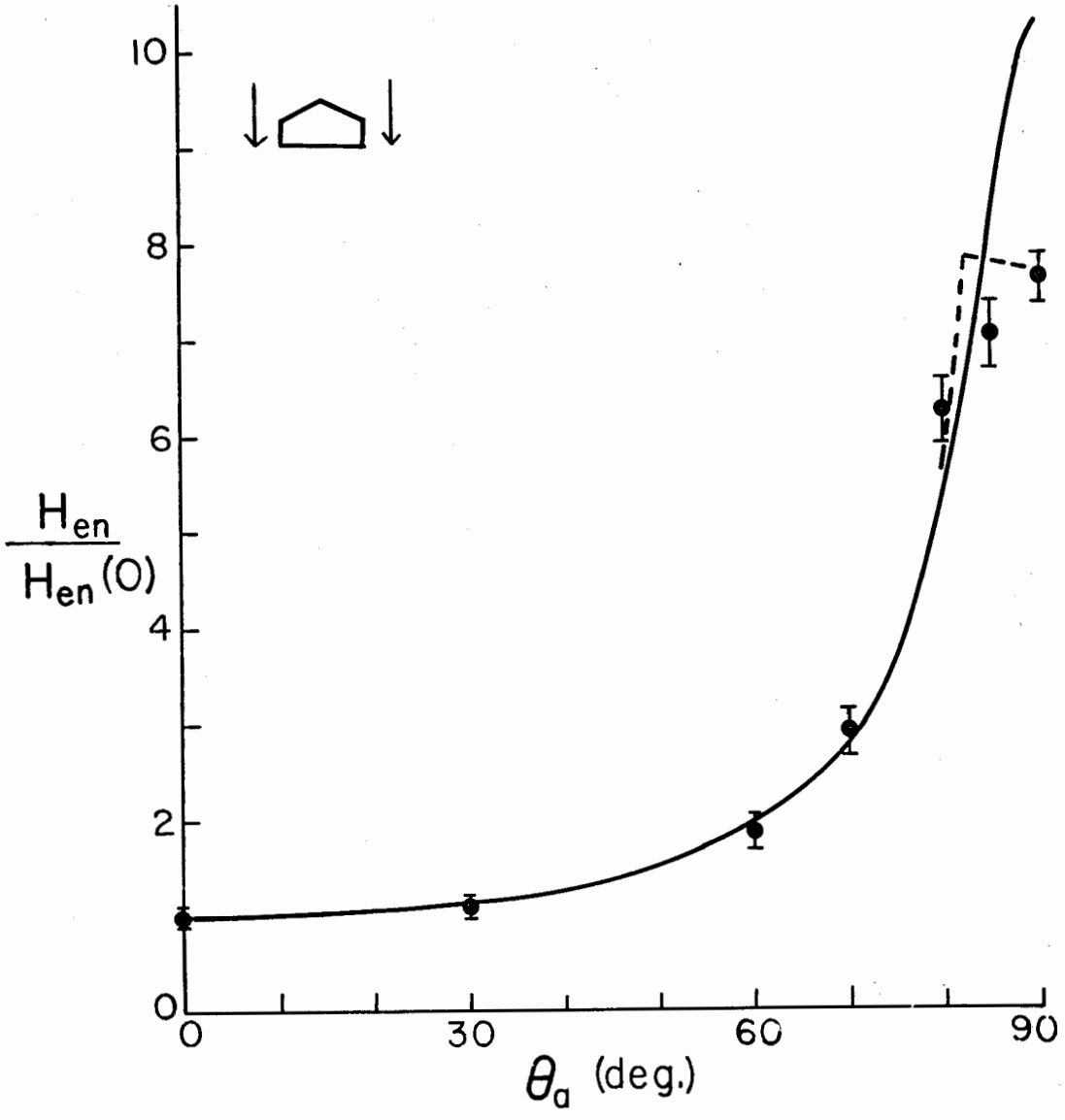

Fig.V.16- Experimental H_{en} data points for $NbSe_2$#3, with h equal to the smaller dimension, compared with Klemm and Clem's theory[1] for $\kappa_\perp$=13.5 and $\sqrt{\epsilon}$=0.25 (solid), and with the parallel/perpendicular model (dashed). The insert shows the direction of the applied field for θ_a=90.

a crystal. Suppose the fluxoids are allowed to lie only perpendicular to the crystal layers or parallel to the layers. Substituting H_{en} for H_{c1} in equation (2-10) and putting $\theta_B=0$ or $\theta_B=90$, gives for H_{en}

$$H_{en}(\theta_a) = \frac{(1-N)\,4\pi F_i/\phi_o}{\cos\theta_a} = \frac{H_{en}(0)}{\cos\theta_a}$$

$$\text{or } H_{en}(\theta_a) = \frac{(1-L)\,4\pi F_i/\phi_o}{\sin\theta_a} = \frac{H_{en}(90)}{\sin\theta_a} \quad , \tag{3}$$

whichever is smaller. $H_{en}(0)$ and $H_{en}(90)$ are the measured values of the entrance field at 0 and 90°. This model is compared with the measured data in Figs.V.13, 14, 15, and 16. Agreement is quite good. The shape of the simple model predicts the shape of the data, except in Fig.V.16. This suggests that the flux lines do enter a crystal either parallel or perpendicular to the layers and not parallel to the external field.

Klemm and Clem's calculation assumes that the fluxoids are symmetric; that is, the shielding currents circle in planes which are perpendicular to the fluxoid axis. In a recent paper, Kogan[23] shows that symmetric fluxoids cannot satisfy the anisotropic London equations. Kogan suggests that the shielding curents stay in the plane of the crystal layers even if the fluxoid is not perpendicular to the layers. From this, he shows that the self-energy should be larger for angles where the fluxoid is not parallel or perpendicular to the crystal layers. The fluxoids would prefer to lie closer to either parallel or perpendicular to the layers than Klemm and Clem predict. This gives theoretical justification to the above conclusion of the simple parallel-perpendicular model.

VI. Summary and Conclusions

Magnetization measurements were used to find the critical field for flux entry into the bulk of superconducting samples. Measurements of H_{en} for samples of Nb48%Ti, after correction for demagnetization, were found to be isotropic as expected. But the measured value of H_{en} was found to be higher than the expected value for H_{c1}. This delayed flux entry is most probably caused by pinning effects and can be qualitatively described by the theory of the critical state.

Measurements of $H_{en}(90)$ and $H_{en}(0)$ for the anisotropic superconductor $NbSe_2$ were larger than the expected values of H_{c1}. As for the Nb48%Ti, flux entry is delayed. Small variations of $H_{en}(90)$ were observed for different crystals and even different orientations of one crystal. An empirical relation between $H_{en}(90)$ and the dimensions of the crystals was found. This has not been explained theoretically but the variations are not due to differences in crystal composition.

The measured angular dependence of H_{en} shows a break or cusp at about $\theta=80^{\circ}$. This result does not agree with the angular dependence of H_{c1} predicted by Klemm and Clem.[1] A simple model, assuming that the fluxoids enter either parallel or perpendicular to the layers, gives qualitative agreement with the observed angular dependence. This would suggest that in the actual crystals there is an effect which causes the fluxoids to lie closer to parallel or perpendicular than Klemm and Clem predict. In a recent paper, Kogan shows that an assumption made by Klemm and Clem is not valid for intermediate angles. The self-energy of a fluxoid at an intermediate angle should be larger than Klemm and Clem's result. This

would cause the fluxoid to lie closer to either parallel or perpendicular to the crystal layers. Finally, H_{en} is not only dependent on H_{c1} but also on the critical current. It is most likely that the critical current in $NbSe_2$ is itself anisotropic. This would also have an effect on the angular dependence of H_{en}.

A motivation of this work was a desire to investigate to what extent low-field magnetic transitions could be used to find superconducting parameters for anisotropic materials. The present experiments show that the strong demagnetizing effects can be taken into account quantitatively. However the determination of H_{c1} and quantities related to it is made complicated by the presence of flux pinning.

The theory of anisotropic superconductors near H_{c1} has not been developed to a satisfactory degree. Developement along the lines Kogan suggests shows promise. In addition, it seems possible to develop a workable temperature-dependent theory of the critical state, by inserting a temperature-dependent critical current. This would allow a determination of both the critical current and H_{c1} of a superconductor from the temperature induced magnetization curves. It is possible that such a critical state theory could explain the variations of H_{en} with crystal size.

Experimentally, it would be interesting to measure H_{en}using crystals of larger anisotropy (for example intercalated layered compounds such as TaS_2(pyridine)). Artificially produced layered materials show much promise in investigations of anisotropic superconductivity.[24] Precise layers of superconducting and non-superconducting materials can be built up by processes such as sputtering or e-beam evaporation. The anisotropy, purity, and shape can be controlled to a much higher degree than in grown

crystals. In such highly anisotropic films it should be even more difficult to place the flux lines parallel to the planes, unless the applied field is lined up precisely. Artificially-produced samples should make it possible to separate, experimentally, the effects of anisotropy and flux pinning. In this way, low field magnetization measurements would be useful in finding superconducting parameters and in explaining the anomalous entrance and movement of flux in anisotropic superconductors.

References

1) R. A. Klemm and J. R. Clem, Phys. Rev. B 21, 1868 (1980).

2) The lower critical field has been measured previously for $NbSe_2$, but only for the field parallel to the layers. See for example, P. de Trey and Suso Gygax, J. Low Temp. Phys. 11, 421 (1973).

3) Superconductivity, edited by R. D. Parks, Marcel Dekker, Inc., New York (1969).

4) A. D. C. Grassie, The Superconducting State, Sussex University Press (1975).

5) P. Moon and D. E. Spencer, Field Theory for Engineers, Van Nostrand, Princeton, N. J. (1961).

6) J. A. Osborn, Phys. Rev. 67, 351 (1945).

7) R. A. Klemm, J. Low Temp. Phys. 39, 589 (1980).

8) R. E. Schwall, G. R. Stewart, and T. H. Geballe, J. Low Temp. Phys. 22, 557 (1976), and references therein.

9) P. de Trey, Suso Gygax, and J.-P. Jan, J. of Low Temp. Phys. 11, 421 (1973).

10) C. P. Bean, Phys. Rev. Letters 8, 250 (1962).

11) W. A. Fietz, M. R. Beasley, J. Silcox, and W. W. Webb, Phys. Rev. 136, A335 (1964).

12) S. H. E. Corporation, 4174 Sorrento Valley Blvd., San Diego, Ca. 92121, U. S. A.

13) O. V. Lounasmaa, Experimental Principles and Methods Below 1 K, Academic Press, London (1974).

14) Norton, Supercon Division, 9 Erie Drive, Natick, Mass. 01760, U. S. A.

15) P. Lorrain and D. R. Corson, Electromagnetic Fields and Waves, W. H. Freeman and Company, San Francisco (1970).

16) M. Denhoff, S. Gygax, and J. R. Long, Cryogenics (1981), in press.

17) S. Gygax and M. Denhoff, to appear in J. Low Temp. Phys.

18) T. P. Orlando, E. J. McNiff Jr., S. Foner, and M. R. Beasley, Phys. Rev. B 19, 4545 (1979).

19) L. J. Neuringer and Y. Shapira, Phys. Rev. 140, A1638 (1965).

20) R. Kershow, M. Vlasse, and A. Wold, Inorg. Chem. 6, 1599 (1967).

21) D. Saint-James, E. J. Thomas, and G. Sarma, Type II Superconductivity, Pergamon Press Ltd., Oxford (1969).

22) J. Finkly and B. S. Deaver Jr., Solid State Comm. 36, 493 (1980).

23) V. G. Kogan, to appear in Phys. Rev. B.

24) S. T. Ruggiero, T. W. Barbee Jr., and M. R. Beasley, Phys. Rev. Lett. 45, 1299 (1980).

Bibliography

C. P. Bean, Phys. Rev. Letters 8, 250 (1962).

P. de Trey, Suso Gygax, and J.-P. Jan, J. Low Temp. Phys. 11, 421 (1973).

M. Denhoff, S. Gygax, and J. R. Long, Cryogenics (1981), in press.

W. A. Fietz, M. R. Beasley, J. Silcox, and W. W. Webb, Phys. Rev. 136, A335 (1964).

J. Finkly and B. S. Deaver Jr., Solid State Comm. 36, 493 (1980).

A. D. C. Grassie, The Superconducting State, Sussex University Press (1975).

S. Gygax and M. Denhoff, to appear in J. Low Temp. Phys.

R. Kershow, M. Vlasse, and A. Wold, Inorg. Chem. 6, 1599 (1967).

R. A. Klemm, J. Low Temp. Phys. 39, 589 (1980).

R. A. Klemm and J. R. Clem, Phys. Rev. B 21, 1868 (1980).

V. G. Kogan, to appear in Phys. Rev. B.

P. Lorrain and D. R. Corson, Electromagnetic Fields and Waves, W. H. Freeman and Company, San Francisco (1970).

O. V. Lounasmaa, Experimental Principles and Methods Below 1 K, Academic Press, London (1974).

P. Moon and D. E. Spencer, Field Theory for Engineers, Van Nostrand, Princeton, N. J. (1961).

L. J. Neuringer and Y. Shapira, Phys. Rev. 140, A1638 (1965).

T. P. Orlando, E. J. McNiff Jr., S. Foner, and M. R. Beasley, Phys. Rev. B 19, 4545 (1979).

J. A. Osborn, Phys. Rev. 67, 351 (1945).

Superconductivity, edited by R. D. Parks, Marcel Dekker, Inc., New York (1969).

S. T. Ruggiero, T. W. Barbee Jr., and M. R. Beasley, Phys. Rev. Lett. 45, 1299 (1980).